Clemson University
TigerPrints

All Theses Theses

8-2023

Augmented Human Inspired Phase Variable Using a Canonical Dynamical System

Timothy Driscoll
tdrisco@clemson.edu

Follow this and additional works at: https://tigerprints.clemson.edu/all_theses

Part of the Biomedical Commons

Recommended Citation

Driscoll, Timothy, "Augmented Human Inspired Phase Variable Using a Canonical Dynamical System" (2023). *All Theses*. 4096.
https://tigerprints.clemson.edu/all_theses/4096

This Thesis is brought to you for free and open access by the Theses at TigerPrints. It has been accepted for inclusion in All Theses by an authorized administrator of TigerPrints. For more information, please contact kokeefe@clemson.edu.

Augmented Human Inspired Phase Variable Using a Canonical Dynamical System

---

A Thesis
Presented to
the Graduate School of
Clemson University

In Partial Fulfillment
of the Requirements for the Degree
Master of Science
Computer Engineering

---

by
Timothy Driscoll
August 2023

Accepted by:
Dr. Ian Walker, Committee Chair
Dr. Ge Lv
Dr. Adam Hoover

Abstract

Accurately parameterizing human gait is highly important in the continued development of assistive robotics, including but not limited to lower limb prostheses and exoskeletons. Previous studies introduce the idea of time-invariant real-time gait parameterization via human-inspired phase variables. The phase represents the location or percent of the gait cycle the user has progressed through. This thesis proposes an alternative approach for determining the gait phase leveraging previous methods and a canonical dynamical system.

Human subject experiments demonstrate the ability to accurately produce a phase variable corresponding to the human gait progression for various walking configurations. Configurations include changes in incline and speed. Results show an augmented real-time approach capable of adapting to different walking conditions.

Acknowledgments

First, I would like to thank Dr. Ge Lv for his support throughout my entire journey. His lab, knowledge, and experience were vital to my success in completing this project. His unwavering support of me and this project over the past two years made everything possible.

Next, I would like to thank both Dr. Ian Walker and Dr. Adam Hoover for taking the time to serve as members of my committee. Specifically, I would like to thank Dr. Walker for allowing me to work outside the ECE department and pursue a project I was passionate about.

I want to extend thanks to the entire Assistive Robotics Laboratory group. Specifically the help and guidance I received from Therese Parr, Miao Yu, Yash Srivastava, and James Rhoads. All these students were supportive in helping me work with the shared lab equipment. I want to acknowledge Dr. Robert Gregg and Kevin Best from the University of Michigan and Dr. Dana Kulic and Tina Wu from Monash University. The conversations I had with both these groups were critical in my understanding of related research and the success of my project.

Lastly, I would like to acknowledge the continued support from all my friends and family. During my studies at Clemson, I was thankful to continually have a strong network behind me, supporting me throughout all my endeavors.

Table of Contents

List of Tables

List of Figures

Chapter 1

Introduction

1.1 Overview

Bipedal locomotion represents movement on two feet. This form of significant locomotion is only found among modern humans [6]. Advancements in medical and technological fields have promoted the need for improvements in human gait analysis. Human gait analysis represents the study of both kinematics and kinetics during bipedal locomotion [7]. Gait analysis and measurement are crucial information for providing feedback to wearable robotics [8] and forms of physical therapy and rehabilitation such as physiotherapy [9]. The human gait is a periodic set of motions that occur to allow for locomotion. A single gait cycle comprises two steps and can be broken into discrete events such as heel strike and toe-off [10]. The phase of gait represents the location within the cycle and progresses from 0% to 100% during a complete cycle.

Various methods have been proposed and tested to represent the gait cycle phase accurately. These different methods have implemented various sensors and techniques to try and produce the most accurate real-time representation. This thesis proposes a new approach to calculating the human inspired phase variable. The new process requires a single IMU sensor to measure the real-time continuous phase variable. A canonical dynamical system (CDS) first proposed in [11] extracts gait phase and frequency information from the thigh angular velocity. The extracted information is then shifted to properly represent the phase of the thigh angle throughout the gait cycle. This approach eliminates the need for robust filtering models to handle signal noise and effectively produces a linear monotonic human inspired phase variable. The experimental results show the algorithm's ability to provide a continuous phase representation of the gait across variable speeds and inclinations.

1.2 Motivation

Although this project is self-contained several different applications are motivating the need, there were two related projects in the Assistive Robotics Laboratory at Clemson. The two projects at Clemson both required real-time gait analysis to control robotic systems. These systems were a lower limb exoskeleton and a full-leg actuated prosthesis. Advanced control algorithms are needed to take human input and appropriately translate it to the system to perform an actuation process.

The exoskeleton is a system that contains two direct current motors located at the hip joint that exert torques to assist the user during walking. The exoskeleton will assist in the form of a torque to help the user either swing their leg forwards or backward. Based on how the subject walks, the exoskeleton needs to dynamically adjust the magnitude of the exerted torque to optimize walking assistance.

Figure 1.1: Two powered hip exoskeletons: MoveX (Shenzhen Enhanced Power Technology CO., Ltd) (left), MoveX with an able-bodied human user (center), and Sportsmate 5 exoskeleton (Enhanced Robotics) with an able-bodied human user (right).

Since the presented exoskeleton is designed to assist in human walking tasks, human-in-the-loop control algorithms are required. A real-time gait phase input is necessary to determine the current torque application. The algorithm must also be continuous and dynamic to capture the entire gait cycle and variance from user to user.

The second system, an actuated full leg prosthesis, also presented a similar control need to the exoskeleton. The prosthesis was designed to actuate and remove the need for a knee joint. The prosthesis would extend and retract throughout the gait cycle to mimic the knee's behavior during gait.

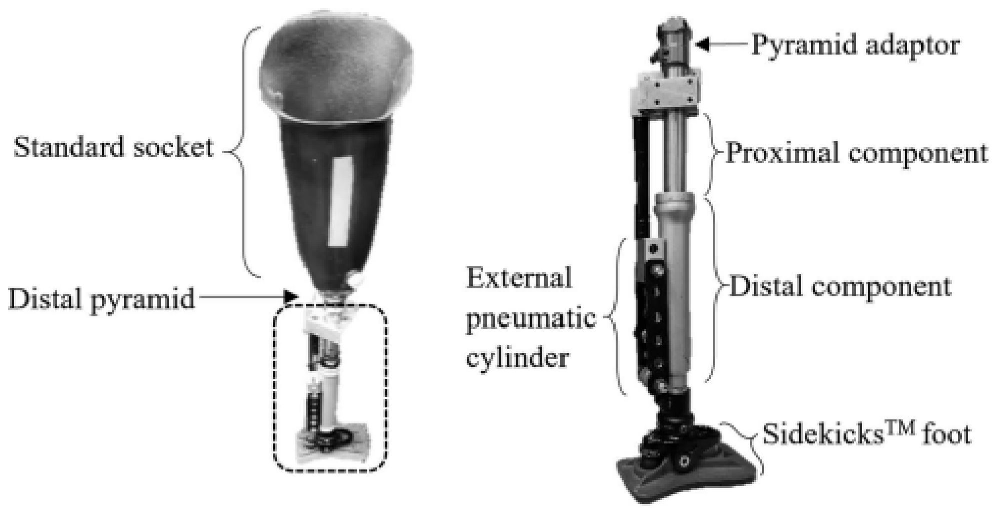

Figure 1.2: Fully constructed linear prosthesis prototype: sagittal view (left) and close-up labeled view (right) [1].

The current control algorithm relies on detecting discrete gait events and predefined timing to actuate the leg during the gait cycle. A force sensitive resistor beneath the foot detects the discrete heel strike and toe-off events during gait. These two events provide limited information but indicate when the gait stance and swing phase start. Figure 1.3 shows the two major gait phases. In figure 1.3 the beginning of the stance phase represents a heel strike, and the start of the swing phase means a toe-off event. A predetermined length of time is then used to segment the series of shortening, lengthening, shortening, and lengthening between two successive heal strikes. The length of time is updated during gait to try and accurately represent how long each cycle takes. In between detected discrete gait events, the control algorithm removes the human from the loop and poses a safety issue if the user were to alter or stop their gait mid-cycle.

The current control algorithm presented for the prosthesis fails to capture the continuous nature of human locomotion and would be vastly improved by a phase variable approach. A phase

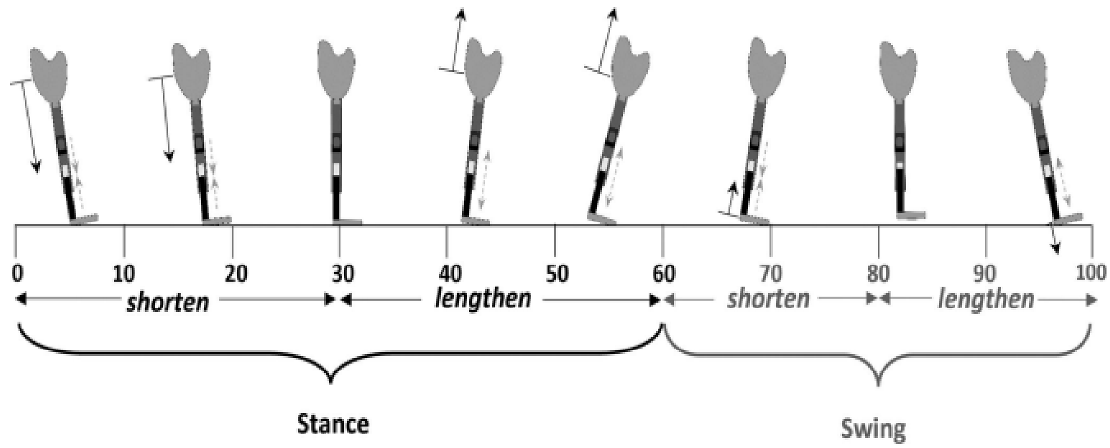

Figure 1.3: Prosthesis length adjustment during stance and swing phase. Representative of the gait cycle ranging from 0% to 100% [1].

variable approach would provide constant real-time information related to the exact percentage of the gait cycle that has been completed. There would be no need for discrete event detection, and continuous tracking would improve overall safety.

The exoskeleton and full leg linear prosthesis need an improved human-in-the-loop control algorithm for gait analysis. Both problems proposed a need for real-time continuous gait cycle analysis. The solution needed to be dynamic and self-contained to provide real-time information to another self-contained system. Improving the control of wearable robots, specifically those designed to aid or enhance locomotion, provided the need and motivation for the development of this project.

1.3 Thesis Overview

The following chapters will present the background information, methods, and testing required to realize an augmented human inspired phase variable approach for real-time gait analysis. Chapter 2 will outline previous research that has contributed to developing gait analysis using wearable sensors. Then chapter 3 will then describe the new algorithm designed to calculate a human inspired phase variable. The hardware used to implement the presented method will be outlined in chapter 4. Chapter 5 outlines the experimental procedure for human subject testing to test the novel design, and the results from the experiments will then be displayed and explained. Finally, the results will be analyzed, and future directions of the work will be discussed in chapter 6.

Chapter 2

Related Work

This chapter will go into detail, discussing the different areas of research that were considered and contributed to the design and development of this project. The different research areas break down the chapter, and various contributions are referenced in each section.

2.1 Sampling Gait

To perform human or bipedal gait analysis, the gait is sampled. Gait sampling is the process of collecting kinetic and kinematic data using external sensors. Kinetics is the study of forces that cause motion and can be observed as the different forces that occur at a human's joints during locomotion (i.e., Hip, Knee, Ankle). Kinematics translates the observed forces into terms such as acceleration, velocity, and position of the human during locomotion. Both the kinetics and kinematics sampled during locomotion are used for gait analysis and control of wearable devices. Various sensors have been used for gait sampling ranging from large-scale camera-based motion capture setups to small wearable sensors such as inertial measurement units.

Large-scale motion capture systems and force plates [12, 13] were commonly used but required expensive equipment and large spaces. Figure 2.1 provides an example of the cameras used and what a typical motion capture would look like, and figure 2.2 shows an example of the needed lab space. In the research community, camera-based motion capture systems are considered the benchmark and are often used to test novel motion tracking approaches [14]. The accuracy and space needed for these large systems make them best suited for clinical gait analysis [15]. Another benefit of these large systems is they can capture a large variety of data such as position, acceleration, speed, and force. Recently, there has been a transition to small wearable sensors for motion capture. This transition has occurred as the need for motion capture has expanded to assistive robotic devices.

Figure 2.1: Vicon motion capture system (Vicon Nexus™): Vicon motion capture camera (left), and representation of motion capture system(right).

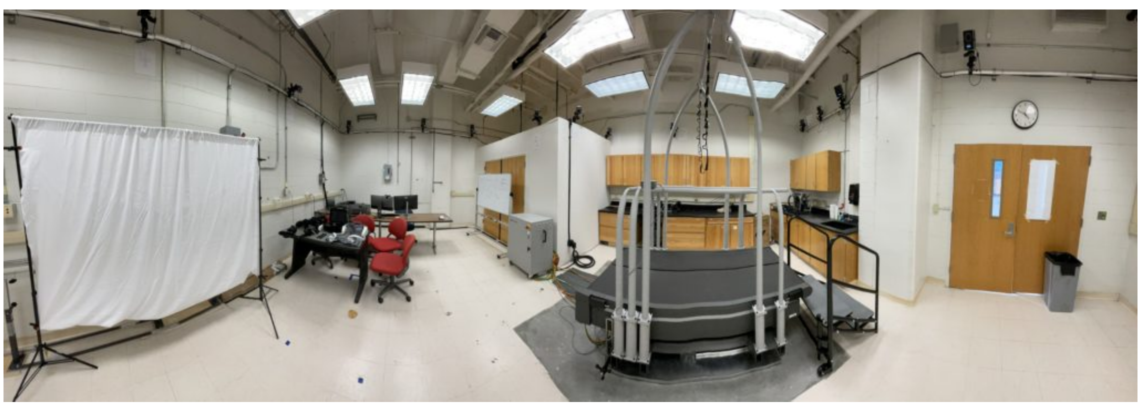

Figure 2.2: Clemson Assistive Robotics Laboratory configured with Vicon Nexus motion capture system.

Small wearable sensors are self-contained, mobile, and easy to use during a variety of different types of analysis. These sensors include IMUs, electromagnetic tracking systems (ETS), electromyography (EMG) sensors, and force sensors such as force sensitive resistors (FSRs) [16, 2, 17, 18, 19]. These sensors can be seen in figure 2.3. These sensors lend themselves to different applications and can be used alone or in conjunction to perform gait sampling. One of the most significant factors in determining the wearable sensors to use during a gait analysis is which gait events will be sampled and what data is trying to be observed. Some sensors, such as FSRs, are only effective at sampling discrete gait events such as toe-off or heel strike. Sensors like an IMU or EMG allow continuous sampling throughout the gait cycle. IMUs are the most common wearable sensor used for gait phase analysis. Most IMUs have 9 degrees of freedom and combine three different sensors into a single package. The three sensors include an accelerometer to measure acceleration forces, a gyroscope to measure angular velocity, and a magnetometer to measure the magnetic field. Typically all three sensors can provide measurements in three directions (X, Y, Z). Algorithms are implemented to fuse data from these sensors and calculate general orientation using Euler angles or quaternions. This often makes IMUs the most appealing wearable sensor for gait sampling. Both [7, 20] select IMUs to measure thigh parameters during gait for phase calculations.

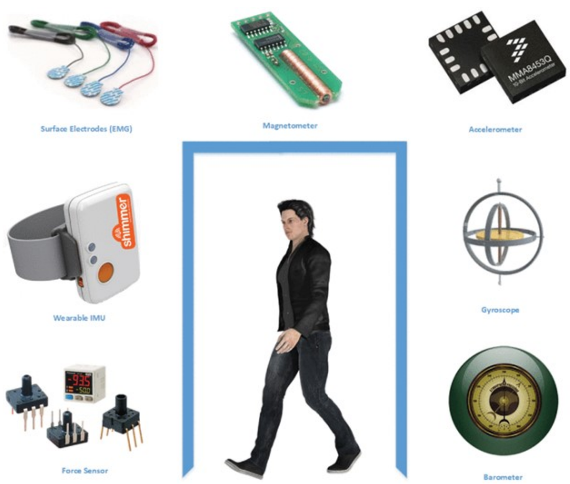

Figure 2.3: Examples of wearable sensors used for gait sampling [2].

2.2 Applications to Sensing Human

When working in the human task space, performing general gait analysis and sampling becomes especially difficult. There can be significant variation in gait when comparing subject to subject. The following studies even show variability in the repeatability of gait from day to day [21, 22]. This makes it challenging to generalize human tasks such as walking a running because there is a significant variation from person to person. Since this is, true generalized methods for human gait analysis are less effective. The gait analysis methods are improved by having real-time adaptability allowing them to be tuned to the specific subject.

In addition to the challenges that variability in gait presents, the other major issue that arises when using wearable sensors to sense human actions is securing and maintaining the position of the sensors. Sensors cannot be mounted to a fixed location but must be adjustable and secure to soft tissue. Since there is no fixed mounting, sensors are subject to movement while being worn, especially during active tasks such as walking. Active tasks also cause additional movement concerns as different muscles activate and flex throughout the task.

2.3 Rule-Based Algorithms for Detecting Gait Classifiers

Rule-based algorithms for detecting gait classifiers rely on discrete gait events to segment the entire gait phase. These algorithms use major gait events such as heel strike and toe-off to break down the gait into different phases, such as stance and swing. The classical gait terms presented in figure 2.4 provide a representation of the discrete events these algorithms work to observe and use to segment the stance and swing phase.

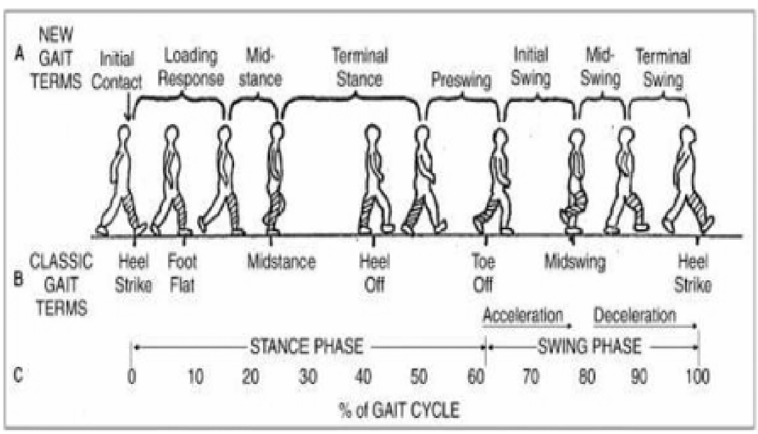

Figure 2.4: Discrete gait events throughout an entire gait cycle [3]. ©2015 IEEE

Sensors such as FSRs are placed in the soles of shoes and are used to detect discrete events [3]. FSRs located beneath the heel and toe allow for heel strike, heel-off, and toe-off to be detected and the gait to be segmented into the swing and stance phase [3]. Similarly, another method combined a gyroscope with the FSRs embedded in a shoe to provide a more dynamic rule-based algorithm. The algorithm implements a state machine, and gyroscope data determines if the gait cycle is disrupted [23]. Other rule-based algorithms for detecting discrete gait events rely on the use of a gyroscope attached to both shanks (shins) [24], or a combination of IMUs attached to the thigh, shank, and top of foot [25]. Patterns detected in the real-time gyroscope data are used to break the gait cycle down into seven different phases [24]. EMGs attached to the right and left thighs have also been used to observe real-time patterns during gait to divide it into seven different phases [26].

These gait phase detection algorithms can effectively segment the gait phase by several discrete events but are often affected by lag and fragile sensors located within the insoles of shoes. Sensors are subject to constant wear and often need to be replaced. These algorithms' biggest con is that they capture the gait phase via discrete events instead of a continuous cycle of motions. They fail to capture the entire gait phase and make assumptions about the motion between discrete events. This flaw makes the presented methods unsuitable for real-world dynamic walking situations, mainly when used to control wearable robotics. Complete and continuous gait awareness is critical when safely controlling wearable robotic devices.

2.4 Phase Variable for Gait Analysis

Dynamic robot locomotion and wearable robotics present new ways of representing and controlling the gait cycle [27]. Most importantly, there has been a shift to representing the gait cycle as a continuous periodic event instead of a series of successive discrete events. The progression of a single variable is mapped to the periodic gait motion to represent the entire gait cycle monotonically. This variable is considered the phase variable and can be used to robustly control the progression of motion when related to quantities such as thigh or ankle position. This variable can be time-invariant and progresses according to its related quantity, allowing it to respond well to different gait interruptions.

Phase variables improved gait analysis techniques by providing a continuous gait representation but were not always time-invariant variables. Some phase variable algorithms still relied on discrete events to mark the beginning and end of the gait cycle. The phase variable was represented by the ratio between elapsed time from the start of the current cycle and the expected cycle duration [28]. Time-dependent methods can be used more reliably for applications in the robotic locomotion task space because a consistent, repeatable series of motions is expected. A time-invariant process is critical to handle inconsistencies and interruptions during natural gait when working in the human sensing task space.

2.5 Human Inspired Phase Variable

Biomechanical research suggested that the hip joint was essential in controlling the two other major joints in the leg [29]. The knowledge that the hip joint had a strong influence in coordinating both the knee and ankle joint made it a strong candidate for relating a phase variable. This research developed the idea of a human inspired phase variable. Relating the phase variable to a quantity, such as a thigh angle, would allow for a time-invariant representation of the gait cycle. The human inspired phase variable would also be robust to real-time changes in gait.

Inspired by biomechanical research, studies observed that thigh motion could uniquely and continuously represent the gait cycle [27]. The gait phase could now be abstracted from a human input such as thigh angle. The research in [27] found that the thigh angle most robustly and uniquely represents the gait cycle. The human inspired phase variable approach solved the previous discontinuous classifier and rule-based algorithms. Groups then focused on accurately capturing and calculating the human inspired phase variable. One of the first real-time continuous gait phase estimations from a single sensor was proposed in [7]. A single IMU sensor was mounted on the test subject's thigh, and the thigh angle was recorded during the gait cycle. The phase variable was then constructed using the phase plane of thigh velocity vs. thigh angle. The thigh angle was reported directly from the IMU, and the thigh velocity was determined by taking the first derivative of the angle. The biggest downfall of the proposed method was sensor noise affected the linearity and monotonicity of the outputted phase variable. To improve the linearity and achieve a monotonic phase variable, filtering the input single and shifting and scaling the phase variable were required. Ultimately, this algorithm does not perform as well with real-time applications because of the inherent noise on the input signal and the inability to post-processing.

Various phase calculations have been implemented to improve the linearity and monotonicity of the human inspired phase variable. One algorithm uses an adaptive frequency oscillator to extract the real-time frequency and phase information [20]. Another recent approach involves using a series of linear equations where the thigh angle remains the input [30]. A finite-state machine controls when each discrete state and corresponding equation to calculate phase is used. Although discrete states exist, the linear equations composing the states ensure that the phase variable calculations are continuous by leveraging prior knowledge about the traditional gait trajectory, the research in [30] significantly improved the linearity and monotonicity of the human inspired phase variable. The improved accuracy comes at the cost of computational complexity and an algorithm that is not as generalizable across various human tasks.

Chapter 3

Methods

The below sections will expand upon the supporting research used to calculate the augmented human-inspired phase variable presented in this paper.

3.1 Human Inspired Phase Variable Calculation

First presented as an offline approach for continuous gait analysis, the idea of using a human inspired phase variable was presented in [31]. This approach required multiple sensors and a combination of the thigh, tibia, and ankle angles. The next iteration of offline analysis proposed using a single human inspired input to parameterize the entire gait cycle using a phase variable. This work found that the thigh angle was the best choice for robustly representing the gait cycle given a single input [27]. This work was later expanded to show proof of a real-time implementation [7]. In these initial implementations, the phase variable was constructed using the phase angle from the thigh phase portrait [7]. The thigh phase portrait is created by plotting the thigh angular velocity (first derivative) by the thigh angle. As the thigh angle changes periodically during the gait cycle, the phase angle orbits a circular revolution with each complete cycle. The phase angle is calculated using the four quadrant $atan2(y, x)$ function [7]. Specifically, the phase angle from the thigh phase portrait would be calculated using the following:

$$\Phi = atan2(\dot{\theta}_{thigh}(t), \theta_{thigh}(t)) \tag{3.1}$$

Where $\dot{\theta_{thigh}}(t)$ and $\theta_{thigh}(t)$ represent the thigh angular velocity and thigh angle respectively. The phase angle calculation presented in 3.1 is not robust to noise and typically results in a phase variable that is neither monotonic nor linear. The $atan2(y, x)$ measures the angle between the positive x-axis and the ray created between the origin and the input (x, y) pair. This calculation makes it imperative that the input thigh angle is a smooth periodic signal to create a circular phase portrait and, ultimately, a linear phase variable. Real-time filtering was used to smooth the thigh angle input in [7], and a monotonic phase variable was produced, but the linearity of the output still was not great, especially at slow walking speeds.

The research presented in [7, 27, 31] proved that a human inspired phase variable could be used to parameterize the gait cycle. The phase portrait algorithm presents a simple phase variable calculation but is not best suited for real-time applications. The noise present in real-time streaming of thigh angle during locomotion prevents a smooth linear phase variable using this approach.

3.2 Canonical Dynamical System

The cons of the phase portrait approach discussed in 3.1 presented the need for an alternative algorithm for extracting phase information from a human inspired input. The algorithm needed to be adaptive to the natural changes in human locomotion and robust to handle the noise present in the input signal. Petrič et al. [11] present a novel algorithm to obtain the phase and basic frequency of an unknown signal with an unknown waveform. The phase and frequency extraction methods are based on adaptive frequency oscillators in a feedback loop. Petrič et al. [11] use a Fourier series representation in a feedback loop combined with a single oscillator.

The canonical dynamical system is a state estimator based on the dynamic Fourier series.

$$\hat{y} = \sum_{c=0}^{M-1} a_{c,t} \cos(c\Phi) + b_{c,t} \sin(c\Phi) \tag{3.2}$$

Where $\hat{y}$ represents the predicted state, a_c and b_c represent the dynamic Fourier series coefficients, M is the number of Fourier series components, and Φ represents the current phase. The Fourier series coefficients are dynamically updated using the following equations:

$$a_{c,t+1} = a_{c,t} + \eta T \cos(c\Phi) e \tag{3.3}$$

$$b_{c,t+1} = b_{c,t} + \eta T \sin{(c\Phi)} e \tag{3.4}$$

Where η is the learning constant, T is the sampling period, and $c = 0, ..., M-1$. Lastly, e is the error signal and is calculated using

$$e = y - \hat{y} \tag{3.5}$$

Where y is the state variable. The adaptive frequency oscillator present in the feedback loop extracts the current frequency and phase from the input signal given the following equations:

$$\omega_{t+1} = \omega_t + T\mu \sin{(\Phi_t)} e \tag{3.6}$$

$$\Phi_{t+1} = \Phi_t + T(\omega_t - \mu \sin{(\Phi_t)} e) \ \% \ 2\pi \tag{3.7}$$

ω represents the estimated angular frequency, and μ represents the coupling constant.

Using the CDS to adaptively model the angular velocity input provided by the IMU's gyroscope allows for the extraction of both gait frequency and phase. This information provides us with real-time speed gait speed estimations and progression traction throughout the gait cycle. Since thigh angular velocity is selected as the human inspired input, phase variable time shifting needs to occur to accurately use the extracted information to represent the phase of the thigh angle.

3.3 Online Time Shifting of the Phase Variable

The phase variable outputted from the equations presented in 3.2 accurately represents the phase of the thigh angular velocity during the gait cycle. This phase variable does not match the phase of the thigh angle during the gait cycle, which is the desired output. The angular velocity was chosen as the input because there was greater repeatability during the gait cycle, the gyroscope has higher accuracy, and the sampling rate could be increased.

The maximum phase variable value is actively tracked to learn the starting and stopping point of each gait cycle and the maximum thigh angle to shift the phase variable dynamically. At this point, the phase variable resets are recorded. The phase variable reset indicates the next thigh angular velocity cycle. The time lag between these two points is determined for each step and saved. The saved time lag from the previous step is then used to shift the current phase variable output. This creates a dynamic time shift and synchronizes the phase variable outputted from the CDS with the thigh angle during locomotion.

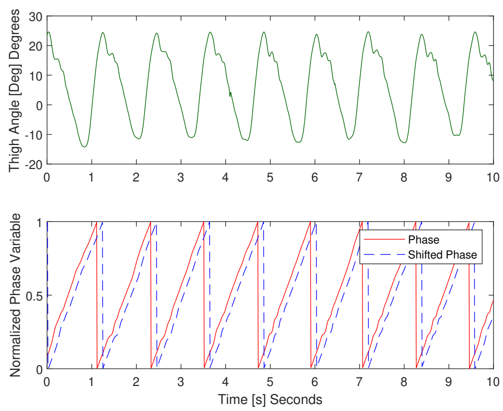

Figure 3.1: Thigh angle (top) and corresponding phase variable (bottom) during locomotion at 1.0 m/s. The dashed line in the bottom graph is the time-shifted representation of the solid line.

Figure 3.1 shows the effects of shifting the phase variable. The shifted phase variable reaches its maximum point (1) when the thigh angle is also at its local maximum. Without any shifting, the phase variable reaches its maximum just before the corresponding thigh angle local maximum. The shifted phase variable can accurately represent the thigh angle phase throughout the gait cycle.

The time-shifted phase variable will take a single gait cycle (two steps) before it can be accurately used to parameterize the gait cycle. A need for information on the previous step causes this brief downtime. Once complete gait cycle will determine the lag between the thigh angular velocity phase and thigh angle. Figure 3.2 shows that the shift takes a single cycle. The phase variable output will remain constant at zero during the first complete gait cycle.

3.4 CDS for Real-Time Gait Phase Estimation

The topics and algorithms presented in the above sections of chapter 3 provide everything needed to complete real-time gait phase estimation. Subsection 3.1 provided evidence that calculating a phase variable for thigh angle would allow us to represent the entire gait cycle uniquely. Subsection 3.2 outlines the algorithm for improved phase variable calculations. The output phase variable is more robust to noise, consistently monotonic, and closely linear. Lastly, section 3.3 pro-

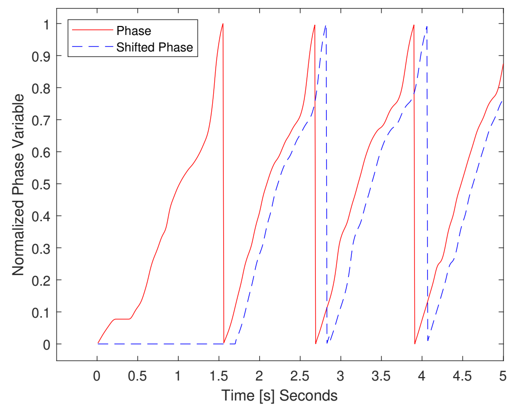

Figure 3.2: Both phase and shifted phase variables during three gait cycles show the time required for the phase shift to be applied actively.

vided the method for appropriately shifting the phase variable to accurately represent the phase of the thigh angle instead of the thigh angular velocity during locomotion.

When combined in a feedback structure, the CDS and time-shifting algorithm can produce an augmented human inspired phase variable in real-time. Figure 3.1 presents the schematic for the phase variable calculation.

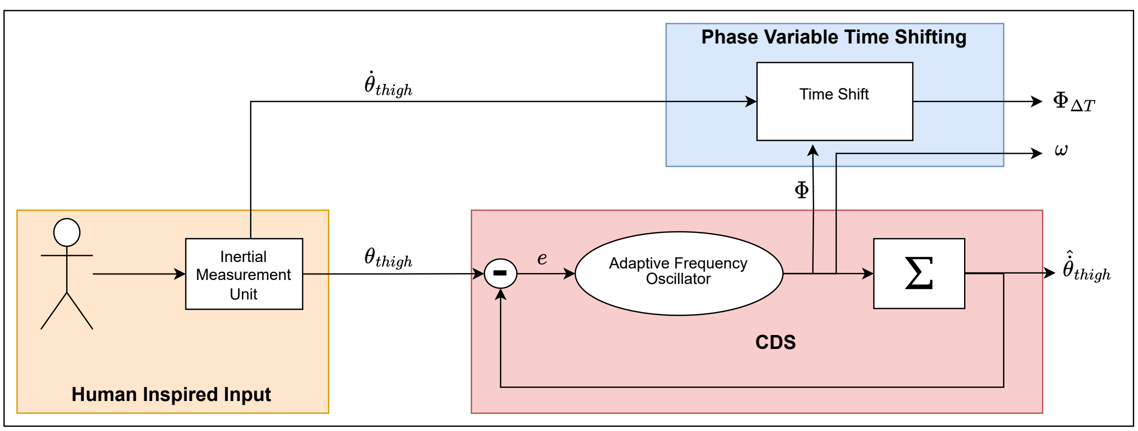

Figure 3.3: Overall diagram of phase variable calculation framework. Broken down into three major subsections, human input (orange), canonical dynamical system (red), and phase variable time shift (blue).

This feedback cycle of predicting, evaluating, and updating was translated into a real-time software application by iteratively implementing the following steps as thigh angular velocity and orientation were streamed from the IMU.

1. Obtain the IMU's current thigh angle and angular velocity measurement.

2. Calculate the current thigh angular velocity state estimate using equation 3.2.
3. Calculate the current error by comparing the state estimation to the IMU measurement using equation 3.5.
4. Update the Fourier series coefficients using equations 3.3 and 3.4.
5. Calculate and extract the updated frequency information by using equation 3.6.
6. Calculate the updated phase variable by using equation 3.7.
7. Extract the time-shifted phase variable.

Steps 1-7 are continuously run, and the sampling frequency of the measurement device dictates the speed. Since the time-shifted phase variable will take a single gait cycle before it can be accurately used to parameterize the gait cycle, two steps must be experienced to begin phase shifting. The extracted frequency also has a convergence period. As the CDS dynamically updates to model the input signal, the frequency converges to a state as steady as the input signal.

Section 5 will provide an experimental procedure and setup testing the algorithm outlined in section 3.4. Results from the experiments will be used to show the effectiveness of the real-time phase estimation algorithm.

Chapter 4

Hardware Implementation

A secondary goal of this project was to realize the phase variable calculations on a self-contained system. The system needed to be mobile and calculate the phase variable in real-time. This chapter will discuss the hardware implementation of the methods presented in chapter 3.

4.1 Inertial Measurement Unit

To create a self-contained mobile gait estimation unit that could be used for various applications, only having a single sensor was a self-defined requirement. A single sensor allows for simple setup, versatility, and no additional coordination for the user. An inertial measurement unit (IMU) can provide the most information in a single package. Typically containing an accelerometer, gyroscope, and magnetometer, they can give individual readings from each sensor and advanced orientation data by fusing all three sensor's data. IMUs also can sense in three dimensions, which is ideal for working in a human task space where motion in three dimensions is expected. An IMU was also well suited for this project because the proposed phase variable calculation depends on thigh angular velocity and angle.

The IMU selected for this project was the Xsens (Movella) MTi-7. This is a 9-degree-of-freedom (DoF) IMU consisting of a three-axis accelerometer, gyroscope, and magnetometer. The IMU is equipped with onboard sensor auto-calibration and a custom fusion algorithm designed by Xsens. The fusion algorithm developed by Xsens combines real-time accelerometer, gyroscope, and magnetometer inputs to output orientation data in the form of roll, pitch, and yaw angles or

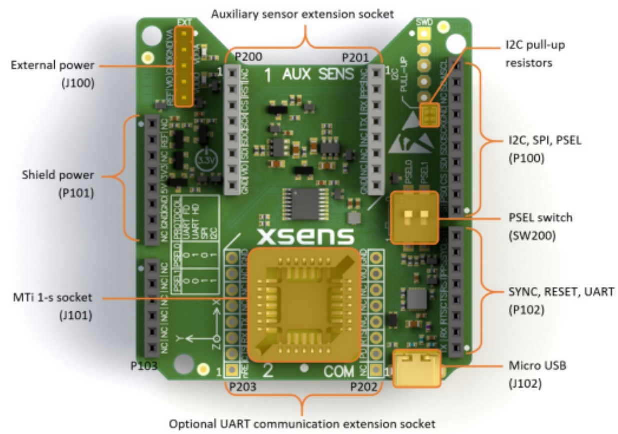

Figure 4.1: MTi-7 development board with labeled connectors [4].

quaternions values. The IMU version purchased for this project included the development board providing pre-soldered connections and a Micro USB port to interface through. The development board can be viewed in figure 4.1 and is approximately 58mm x 54mm and weighs about 3 grams. Table 4.1 summarizes the main features considered when deciding which IMU to purchase. Benefits such as onboard sensor fusion made the Xsens line of IMUs strong candidates. Ultimately, balancing cost and sensor accuracy was the most significant deciding factor.

Specification	Performance
Roll, Pitch Accuracy	0.5 deg RMS
Yaw Accuracy	1.5 deg RMS
Gyroscope Full Range	2000 deg/s
Gyroscope Noise Density	$0.003\ ^\circ/\mathrm{s}/\sqrt{\mathrm{Hz}}$
Accelerometer Full Range	16 g
Accelerometer Noise Density	$70\ \mu\mathrm{g}/\sqrt{\mathrm{Hz}}$
Magnetometer Full Range	$+/-$ 8 G
Magnetometer Noise	0.5 mG RMS
Power Consumption	<150 mW @ 3V
Output Frequency	100 Hz
Cost	$450

Table 4.1: Summary of MTi-7 IMU specifications and corresponding performance.

4.2 Microprocessor

The second major component needed to implement the gait phase algorithm was a microprocessor to perform the data polling, processing, and calculations. Similar to the IMU, the goal of keeping the system small and portable remained a necessary restriction when selecting a microprocessor. To prove this idea, it was essential to perform all data processing on something other than a personal computer. A microprocessor was chosen over a microcontroller for quicker implementation and prototyping. A smaller application-specific controller could be designed and used in future deployments.

Ultimately, a Raspberry Pi 4 Model B with 4GB of RAM was selected to be the microprocessor for the project implementation. The Raspberry Pi is a powerful minicomputer configured with Raspberry Pi OS, a Linux-based operating system. The Raspberry Pi is also configured with various communication peripherals such as USB/UART, SPI, and I^2C, making it well suited for prototyping. The Raspberry is also configured with a display port and can connect a monitor, keyboard, and mouse for development ease. Figure 4.2 shows the Raspberry Pi used for development configured with a hard plastic case and fan for cooling.

Figure 4.2: Raspberry Pi 4 B microprocessor with CanaKit housing and fan [5].

4.3 Sensor Communication

The IMU transmitted real-time data to the Raspberry Pi using serial communication. The serial communication was implemented by way of USB, and USB to UART converters were used to read the serial data on both sides. The USB connection provided the IMU with 5V and a data transmission rate of 115200 baud. Additionally, the PySerial library was used to provide communication support. Although serial communication is not the quickest option available on the IMU, it offered a simple connection via USB and was optimal for prototyping. Since the data was only being streamed at 100 Hz, the serial communication effectively handled the data transmission. Lastly, serial communication was chosen to allow for a seamless transition from development on PC to trials using the Raspberry Pi. In future project implementation, transitioning to SPI or I^2 communication would improve data transition rates and security. SPI communication would also eliminate potential mismatches between the transmitter and receiver clocks.

The Xsens IMU transmits data serially using a binary communication protocol called the Xbus protocol. The IMU operates in two different states a configuration and a measurement state. The configuration state is used to both get and set the IMU settings. These settings include but are not limited to desired data output, sampling frequency, and baud rate. The IMU was configured to transmit both orientation and gyroscope data at a frequency of 100 Hz. The baud rate was set to 115200 Bps which is the maximum supported by the Raspberry Pi. Once set, a configuration message will be sent to the host just before entering the measurement state. In the measurement state, an MTData2 message containing the configured IMU data is continuously transmitted. Figure 4.3 shows the message configuration. The Xbus header provides four bytes of data indicating the data's start, identification, and length. The configured data can range from 0-254 bytes depending on the desired outputs and settings. Lastly, a single-byte checksum is included to determine if any errors in the message were incurred during transmission.

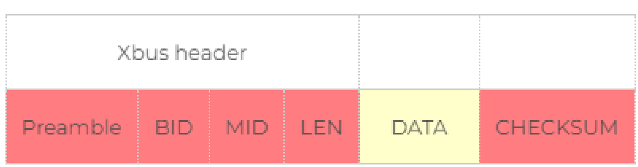

Figure 4.3: An MTData2 message configuration using the Xbus protocol [4].

4.4 Software Development

All sensor communication, processing, and phase variable calculations were written in Python 3. A high-level interpreted language was chosen to develop the software to continue and allow for rapid prototyping. A standalone library for low-level communication with the Xsens [32] was modified and used to interface the IMU with the Raspberry Pi. The library provided source code for configuring the IMU, reading Xbus messages, and extracting the data in a readable format. On top of this library, code was developed to perform real-time phase variable calculations and track the gait cycle. Using Python, the real-time measurements and calculations were recorded and written to a CSV file for data analysis. In addition to the Python scripts written for real-time processing and calculations, MATLAB scripts were written to extract data and perform analysis. No additional offline scripts were used to process the data, only to manipulate and view the results. Future software implementations would benefit from transitioning to a precompiled language for faster speeds and a more optimized approach. C++ would be the language of choice when making this transition.

4.5 IMU Verification and Benchtop Testing

For the algorithm presented in chapter 3, the IMU was required to provide both orientation and angular velocity. As discussed in section 4.1, the selected IMU could produce an orientation using onboard sensor fusion algorithms. The orientation extracted was the IMU pitch angle, corresponding to the angle of the subject's thigh in the sagittal plane. Figure 4.4 provides an example of the IMU output that tracks the thigh angle. The average thigh angle with respect to time is also displayed. The angular velocity used for the phase calculation corresponded to the rotation around the z-axis. This rotation was read directly from the gyroscope, and an example can be observed in figure 4.5. Both signals are relatively smooth but experience noise when the foot meets the ground during each gait cycle. The foot contact can be observed around 0.2 seconds of the right graph in both figures 4.4, and 4.5.

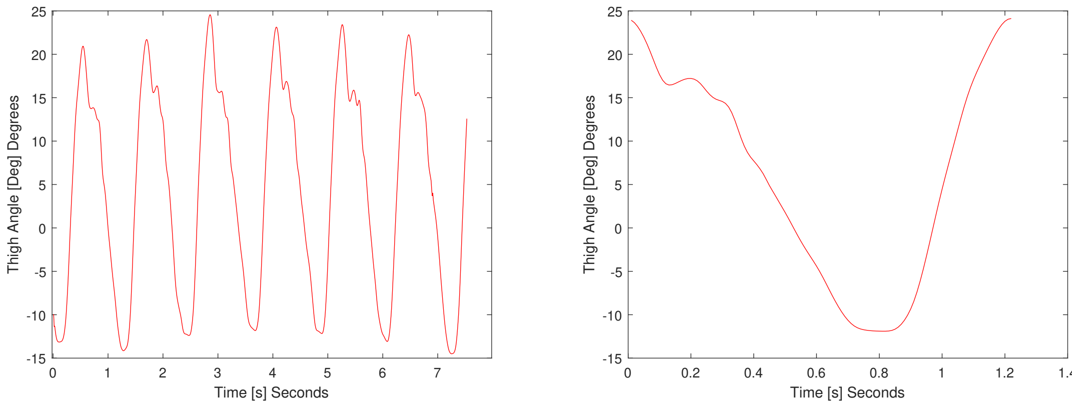

Figure 4.4: Raw inputs of the thigh orientation with respect to the sagittal plane streamed from the IMU. Continuous thigh angle from the first five steps of subject AB01 walking on level ground at 1.0 m/s (left). Average thigh angle throughout the gait cycle during the 30-second walking period on level ground at 1.0 m/s (right).

4.6 Interface for Human Sensing

To use the IMU as the sensor for the human-inspired input, it needed to be secured to the test subject's thigh. The sensor needed to be connected in an adjustable way and could be used across a range of test subjects. A flexible fabric strap with Velcro was used to secure the IMU to the subject's mid-thigh. A case was designed and 3D printed to secure the IMU to the strap and comfortably allow the IMU to be oriented on the side of the subject's thigh. The case provided pin slots for the development board peripheral pins and nested bolt locations to secure the IMU. Figure 4.7 shows the IMU mounted to three test subjects. All subjects could use the same leg strap and incurred reduced movement during gait.

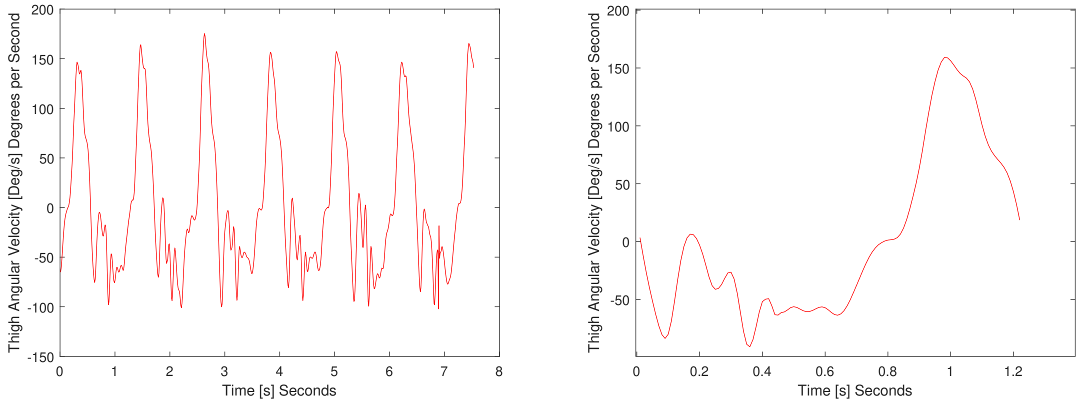

Figure 4.5: Raw inputs of the thigh angular velocity in the sagittal plane streamed from the IMU. Continuous thigh angular velocity from the first five steps of subject AB01 walking on level ground at 1.0 m/s (left). Average thigh angular velocity throughout the gait cycle during the 30-second walking period on level ground at 1.0 m/s (right).

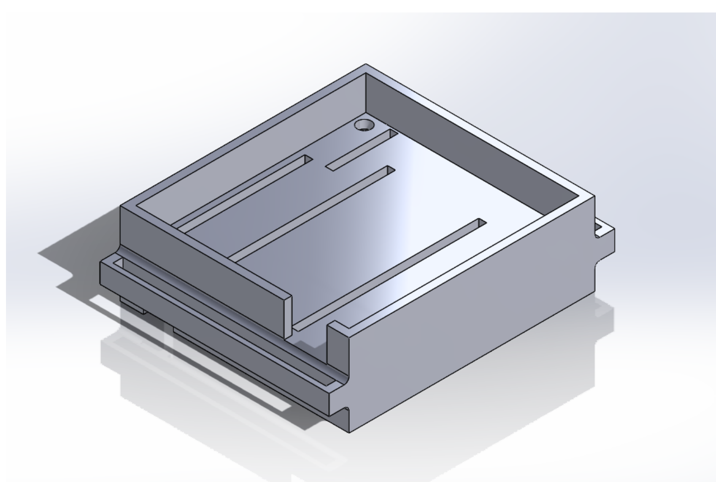

Figure 4.6: 3D model of IMU case used to mount IMU to human subject's thigh.

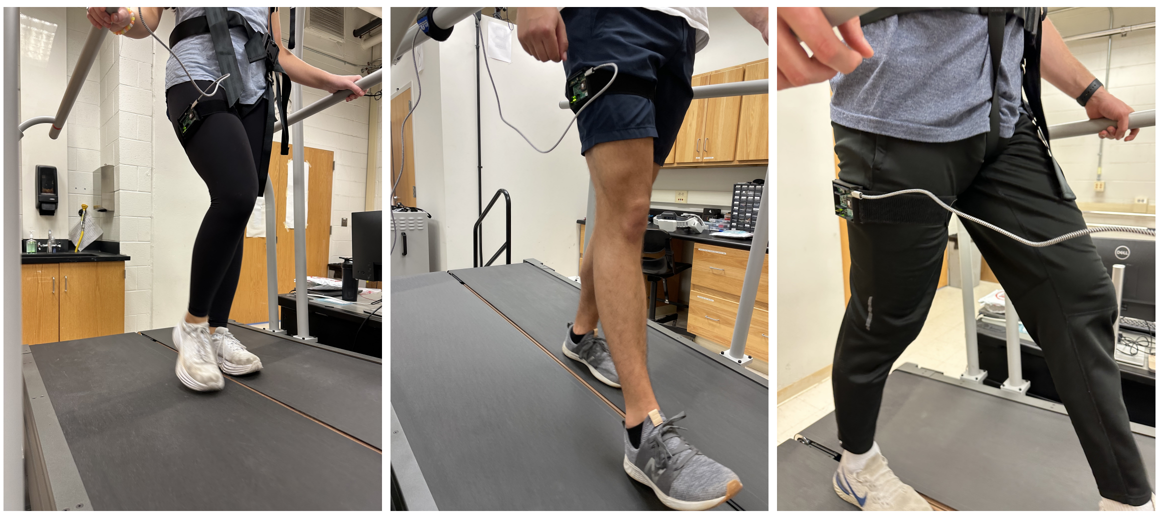

Figure 4.7: Subjects AB01, AB02, and AB03 (left to right) walking with the IMU mounted during experimental trials.

Chapter 5

Experiments and Results

In this section, we demonstrate the benefits of the CDS phase variable approach via a series of human-subject walking experiments. The experiments were conducted to test the approach under a variety of different walking conditions by varying speed and incline. An outline of the experimental protocol will be given, and then corresponding results will be presented.

5.1 Institutional Review Board

To accurately test the effectiveness of the new phase variable approach, human subjects were required. Human subjects would allow for an accurate use representation in a controlled testing environment. Since human subjects were required, an experimental protocol needed to be submitted to the Institutional Review Board (IRB) at Clemson University. A screening document, consent form, data collection tools overview, and recruitment were all submitted to the IRB. The screening document was used to determine if willing participants met the physical qualifications to participate in the experiment. The consent form provided a complete experiment outline and provided potential candidates with all the information necessary when making a decision to join or not. The data collection tools overview gave a complete outline of all the tools and devices that were or could be used during the experimental trial. Finally, the recruitment script was used to email potential candidates and gain an interest in participating. Multiple rounds of revisions were required before receiving final approval. The protocol was approved under case number IRB2022-0735, allowing for human subject testing. Along with completing the experimental protocol and gaining IRB approval, I was also required to complete and pass the Collaborative Institutional Training Initiative (CITI Program) "Human Subjects Protection Course."

5.2 Experimental Protocol

The relevant details of the approved IRB protocol will now be outlined. To gain confidence in our results, six different participants (3 female/3 male) were selected to complete the following series of tests. Each test consisted of a single participant walking on a treadmill with the IMU mounted on their thigh. The IMU was mounted on the thigh along the subject's sagittal plane. The subject was then tasked with walking at five different inclines at three different steady speeds. The inclines included 0 degrees, +/- 5 degrees, and +/- 10 degrees. At each one of these inclines, the subject would walk at 0.67 m/s, 1.00 m/s, and 1.35 m/s for 30 seconds each. Additionally, at each incline, the user would be recorded walking over a series of two-speed transitions. The speed transition included 20 seconds of walking at 0.67 m/s, then 20 seconds of walking at 1.35 m/s, finally followed by 20 seconds at 0.67 m/s. In total, each subject was recorded walking in 20 different configurations of speed and incline. To most accurately capture the subject's normal gait, they were given time to normalize their gait in each prior to beginning the data collection period. After completion of the data collection in the given configuration, the user was given a rest prior to transitioning to the next configuration. Each subject trial was completed in approximately two hours, and 120 different walking samples were recorded.

5.3 Algorithm Parameters

When performing trials, there are a number of different algorithm parameters that need to be initialized. Table 5.1 summarizes how all the parameters were defined at the start of each trial. The sampling frequency was predetermined by the constraints of the IMU and was adjusted to reflect the maximum frequency. The next three parameters, M, η, and μ, were all tuned after preliminary trials to promote quick frequency and phase convergence. The frequency was predefined by using prior knowledge of the gait cycle period at a normal walking speed. The gait cycle period was estimated to be about 1.25 seconds, resulting in a frequency of 0.8 Hz. This frequency was then converted to angular frequency by multiplying by 2π. Finally, the last three parameters were

Parameter	Initial Value
Sampling Frequency [T]	100 Hz
Number of Fourier Series Coefficients [M]	7
Learning Coefficient [η]	1
Coupling Constant [μ]	0.1
Frequency [w]	$0.8 * 2/\pi$
Phase [Φ]	0
a_c	0 for $c = 0, ..., M-1$
b_c	0 for $c = 0, ..., M-1$

Table 5.1: Definition of all the initial parameters required to compute the phase variable.

initiated to zero because no prior knowledge was available to adjust the initial value.

5.4 Results

The results subsection will be used to present a series of results in the form of graphs. All phase variable calculations were performed in real-time during human subject walking experiments. The outputted results were saved and plotted using MATLAB. The only additional post-processing performed in MATLAB was calculating averages and standard deviation of the phase variable across the entire trial period.

5.4.1 Phase Variable Output

The first series of data represented by figures 5.1, 5.2, and 5.3 contains a total of 18 plots. These plots represent the average phase variable over the 30-second walking period for three different speeds. Each individual plot corresponds to a specific test subject, and each figure corresponds to the different walking inclines (level ground, 10 degrees, -10 degrees). The shaded region around each plot provides the phase variable standard deviation. The phase variable was normalized to range from 0 to 1 during each gait cycle. The x-axis is seconds and was not normalized with respect to time to range from 0 to 100 percent of the gait cycle. The x-axis was chosen to be displayed in time so the change in walking speed could be reflected by each graph.

Figure 5.1 and its corresponding summary table 5.2 display the obtained phase variable results from all subjects walking on level ground. Through the graphs, the three different speeds can be observed by the change in slope between all three lines. It can also be observed that there was a decrease in the time when the phase variable reached one as the speed increased. Across all subjects and speeds, the maximum average standard deviation was 0.1794, and the overall maximum was 0.3147. Across all subjects and speeds, the maximum standard deviation usually occurred around $0.25 - 0.40$, having a strong correlation to foot contact and an added spike in noise.

Subject	Standard Deviation at 0 Degrees								
	0.67 m/s			1.0 m/s			1.35 m/s		
	Avg	Max	Time	Avg	Max	Time	Avg	Max	Time
AB01	0.1105	0.1641	0.73	0.1143	0.2037	1.05	0.1479	0.2683	0.36
AB02	0.1786	0.3147	0.46	0.1136	0.2088	0.39	0.1143	0.2059	0.92
AB03	0.1488	0.2246	0.41	0.1496	0.2477	0.39	0.1311	0.2788	1.04
AB04	0.1565	0.2512	1.12	0.1794	0.3045	0.44	0.1252	0.2576	0.95
AB05	0.1400	0.2339	0.46	0.1428	0.2780	0.38	0.1677	0.3108	0.35
AB06	0.1519	0.2214	0.45	0.1132	0.2100	0.36	0.1387	0.2619	0.32

Table 5.2: Summary table of the phase variable standard deviation for all subjects walking on level ground. For all three trial speeds, the table includes the average standard deviation, maximum standard deviation, and time at which the maximum standard deviation occurs.

Figure 5.2 and its corresponding summary table 5.3 display the obtained phase variable results from all subjects walking on a 10-degree incline. The graphs again show an increase in slope with an increase in speed. Across all subjects and speeds, the maximum average standard deviation was 0.1592, and the overall maximum was 0.3267. Across all subjects and speeds, the maximum standard deviation also usually occurred around $0.25 - 0.40$, having a strong correlation to foot contact and an added spike in noise. In a few instances, the maximum occurred closer to the end of the gait cycle.

Subject	Standard Deviation at 10 Degrees								
	0.67 m/s			1.0 m/s			1.35 m/s		
	Avg	Max	Time	Avg	Max	Time	Avg	Max	Time
AB01	0.1130	0.2032	0.39	0.1457	0.2529	0.34	0.1197	0.2564	0.32
AB02	0.1556	0.2288	1.12	0.1158	0.2328	0.37	0.1316	0.2478	0.33
AB03	0.1579	0.2864	1.39	0.1592	0.2900	1.14	0.1523	0.3267	1.02
AB04	0.1249	0.1870	1.22	0.1255	0.2345	1.19	0.1270	0.2803	1.00
AB05	0.1450	0.2794	0.38	0.1146	0.2177	0.37	0.1362	0.2940	0.35
AB06	0.1505	0.2107	0.36	0.1168	0.2190	1.04	0.1406	0.2914	0.35

Table 5.3: Summary table of the phase variable standard deviation for all subjects walking at a 10-degree incline. For all three trial speeds, the table includes the average standard deviation, maximum standard deviation, and time at which the maximum standard deviation occurs.

Finally, the last figure in the first set, figure 5.3 and its corresponding summary table 5.4 display the obtained phase variable results from all subjects walking on a 10-degree decline. The graphs again show an increase in slope with an increase in speed. Across all subjects and speeds, the maximum average standard deviation was 0.2820, and the overall maximum was 0.5583. This walking configuration produced both the highest average and maximum standard deviation. Across all subjects and speeds, the maximum standard deviation also usually occurred around $0.25 - 0.45$, having a strong correlation to foot contact and the period directly after.

Subject	Standard Deviation at -10 Degrees								
	0.67 m/s			1.0 m/s			1.35 m/s		
	Avg	Max	Time	Avg	Max	Time	Avg	Max	Time
AB01	0.2722	0.4648	0.41	0.2508	0.4739	0.39	0.2370	0.3979	0.24
AB02	0.1873	0.3488	0.48	0.1499	0.2931	0.38	0.1413	0.2576	0.30
AB03	0.2576	0.4582	0.53	0.2036	0.3574	0.39	0.2820	0.4711	0.33
AB04	0.2416	0.4208	0.36	0.2488	0.4814	0.27	0.1913	0.4031	0.24
AB05	0.1959	0.3489	0.46	0.2748	0.4904	0.42	0.2191	0.4373	0.32
AB06	0.3022	0.5583	0.52	0.2181	0.4276	0.37	0.2065	0.4479	0.35

Table 5.4: Summary table of the phase variable standard deviation for all subjects walking at a 10-degree decline. For all three trial speeds, the table includes the average standard deviation, maximum standard deviation, and time at which the maximum standard deviation occurs.

5.4.2 Phase Variable Comparison

The second series of data represented by figures 5.4, 5.5, 5.6, and 5.7 presents the phase variable performance during transitions in comparison to a traditional phase variable calculation approach. Each row of plots represents a continuous walking trial where two transitions occurred. In the leftmost column, the subject is walking at 0.67 m/s. In the middle column, they transition to walking at 1.35 m/s, where the acceleration is 0.1 m/s^2. Finally, in the rightmost column, the subject transitions back to walking at 0.67 m/s, where the deceleration is 0.1 m/s^2. The data presented in this section only includes walking at level ground and a 10-degree incline. The 10-degree decline was not included because the traditional phase variable approach performed poorly and was hard to interpret. The six subjects are split across two figures for both walking configurations.

The traditional phase variable in the comparison figures was calculated using the phase portrait method presented in 3.1. An additional smoothing parameter was used to optimize the linearity of the traditional phase variable [27]. The traditional phase variable was not calculated in real-time, and the required information was not available in real-time to perform smoothing.

Figures 5.4 and 5.5 represent the level ground walking results. This paper's CDS phase variable approach shows a consistent smooth monotonic across all transitions. Whereas the traditional phase variable approach is far less smooth and, in certain cases, is not monotonic. It should also be noted that the traditional approach is held constant at 0 for 0.3 seconds. This was done to prevent further disruption in monotonicity from foot contact. The CDS phase variable shows minor disturbances from foot contact but remains monotonic throughout the entire gait cycle,

Similarly, figures 5.6 and 5.7 represent the level ground walking results. Again the CDS phase variable handles all transitions and remains smooth and monotonic. Whereas the traditional phase variable needed to be constant for the first 15 seconds to remove disturbances from foot-to-ground contact. The traditional phase variable shows the most consistent results towards the end of the gait cycle during the swing phase, with no ground contact from the leg being measured.

5.5 Discussion

Overall, the proposed method for phase variable calculation performed strongly for all six subjects and across all 20 different walking configurations. The outputted phase variable was always monotonic and provided a smooth linear result to segment the entire gait cycle.

The phase variable was consistent across each respective walking task. The standard deviation across all subjects at level ground was 0.1402. At 10 degrees, the standard deviation was 0.1351; finally, at -10 degrees, it was 0.2267. Across all subjects and configurations, the average standard deviation was 0.1673. This showed steady consistency during the repetitive gait tasks as desired. Walking at a decline created the most significant variance in phase variable calculations. This walking task was the most unnatural for subjects and resulted in a more unsteady gait, as reflected by the standard deviation. Multiple subjects noted feeling unnatural at a decline on a treadmill. The most inconsistent portion of the phase variable occurred from 0 to 0.5 or the first fifty percent of the gait cycle. At this point in the gait cycle, the foot corresponding to the leg being measured (right) was in contact with the ground (treadmill). Noise from the heel striking and inconsistent movements from the opposite foot's toe off can likely account for this noise. Additional input signal filtering would handle some of this noise and further smooth the phase variable.

The second significant result presented in this thesis is a comparison to previous phase variable approaches. The original human-inspired phase variable approach was used as a benchmark for comparing the proposed method. The original method was calculated using the $atan2$ function and the phase portrait. This comparison was made during the walking configuration that included multiple speed transitions. The comparison was made during this series of tests to highlight the adaptability of the new approach. Viewing the comparison plots, it is evident that the CDS approach outperforms the traditional approach. There is a significant improvement in the phase variable's linearity, monotonicity, and consistency. Additionally, the CDS approach was purely calculated in real-time. Relying on the phase portrait causes monotonicity issues when noise is experienced. Given the nature of the $atan2$ function, if there is an unexpected increase in the thigh angle while it should be following a steady decrease, rapid jumps in the phase variable will occur. Since the CDS approach relies on modeling the state variable, inconsistent noise doesn't result in significant phase variable error or change.

It is important to note that although the phase portrait method for calculating the phase variable was used as a benchmark, it is not the most current phase variable calculation being implemented. A continued effort has been made to improve the reliability and performance of phase variables. Further evaluation and comparison of the CDS approach are still required. The results for the method presented in this thesis show strong promise in the overall effectiveness of this approach.

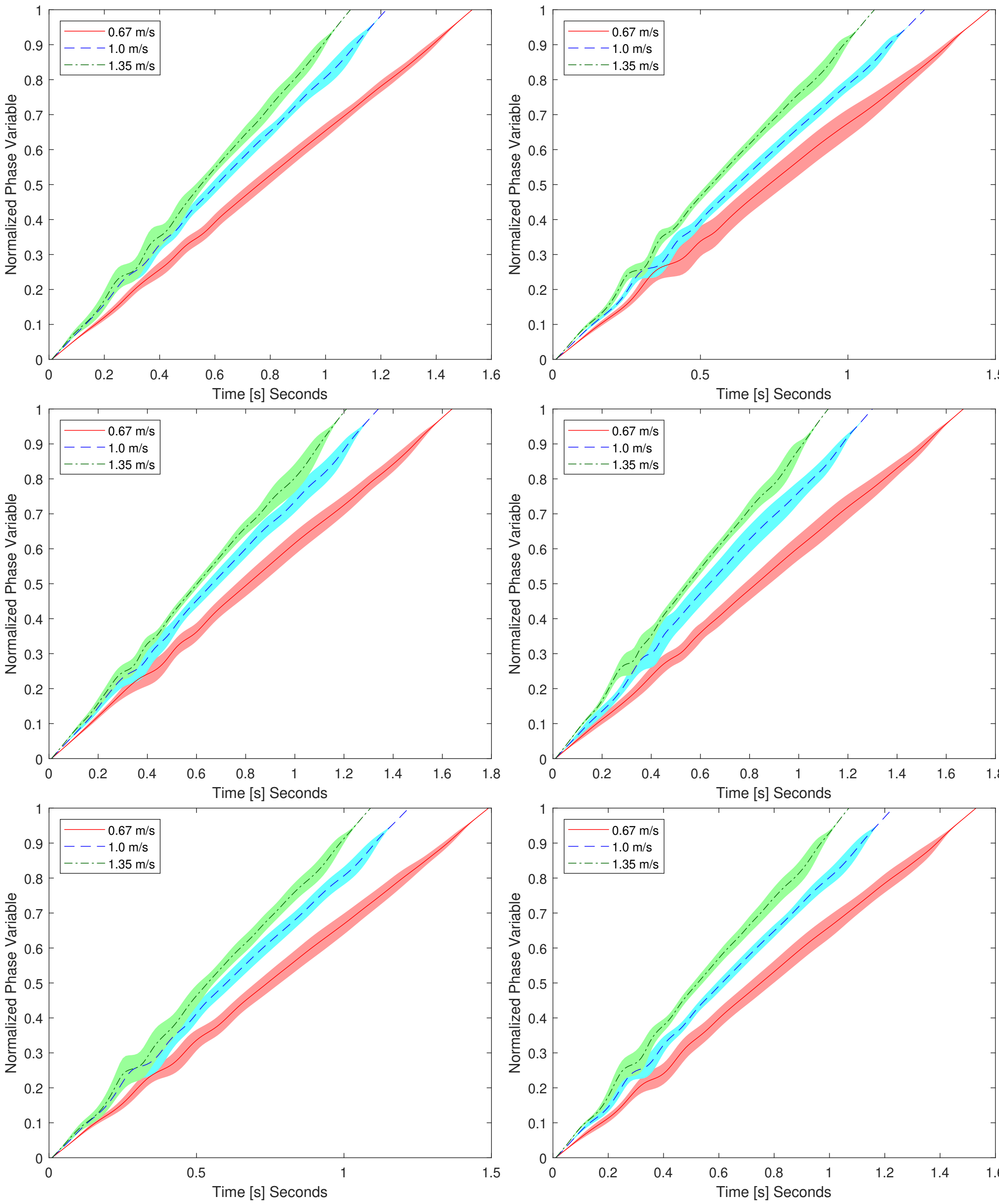

Figure 5.1: Reading from top to bottom, left to right normalized phase results for test subjects 1-6 at walking on level ground at the three different trial speeds. The lines provide the average normalized phase variable throughout the gait cycle, and the shaded region is the standard deviation over the 30-second trial period.

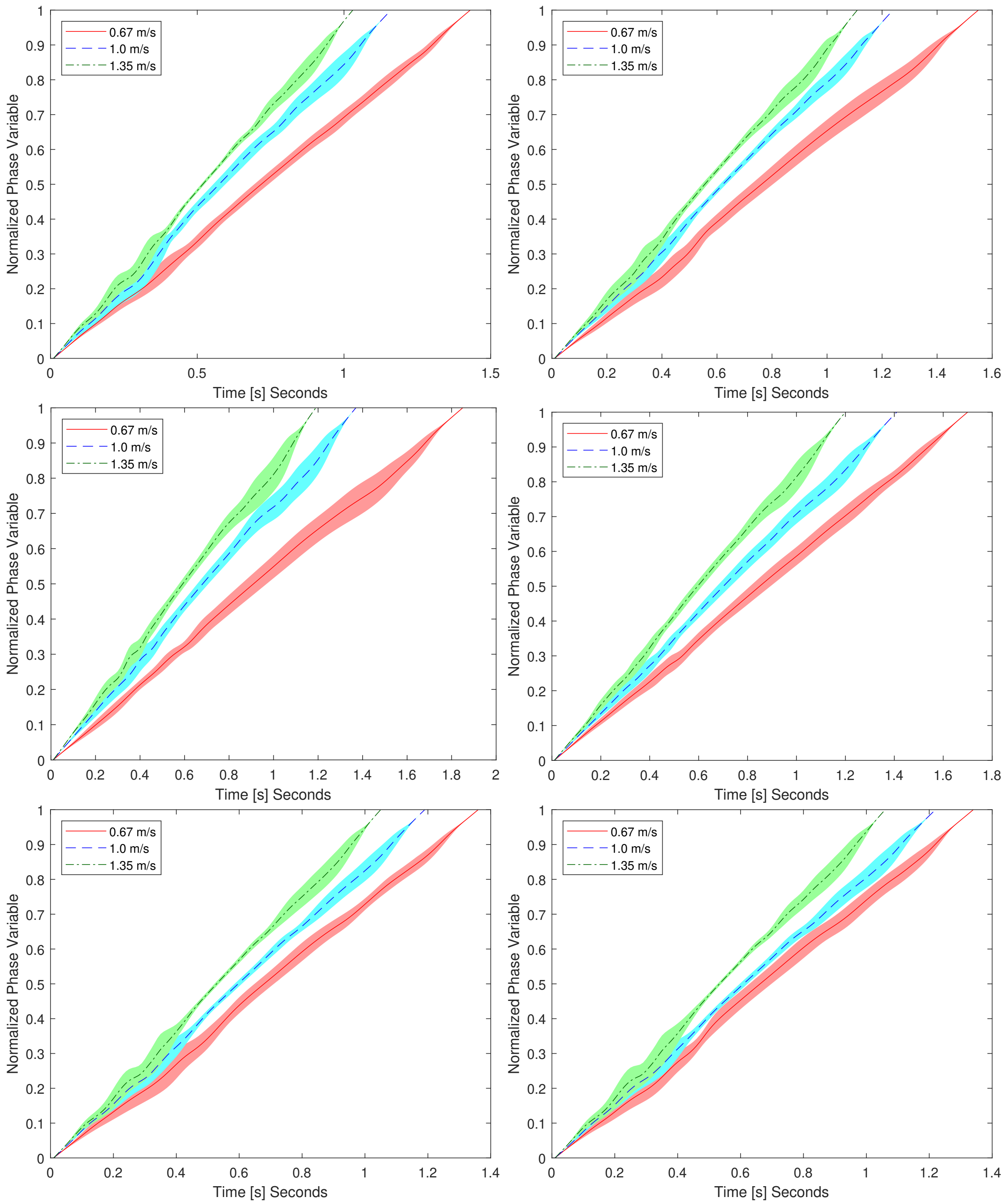

Figure 5.2: Reading from top to bottom, left to right normalized phase results for test subjects 1-6 walking at a 10 degree incline at the three different trial speeds. The lines provide the average normalized phase variable throughout the gait cycle, and the shaded region is the standard deviation over the 30-second trial period.

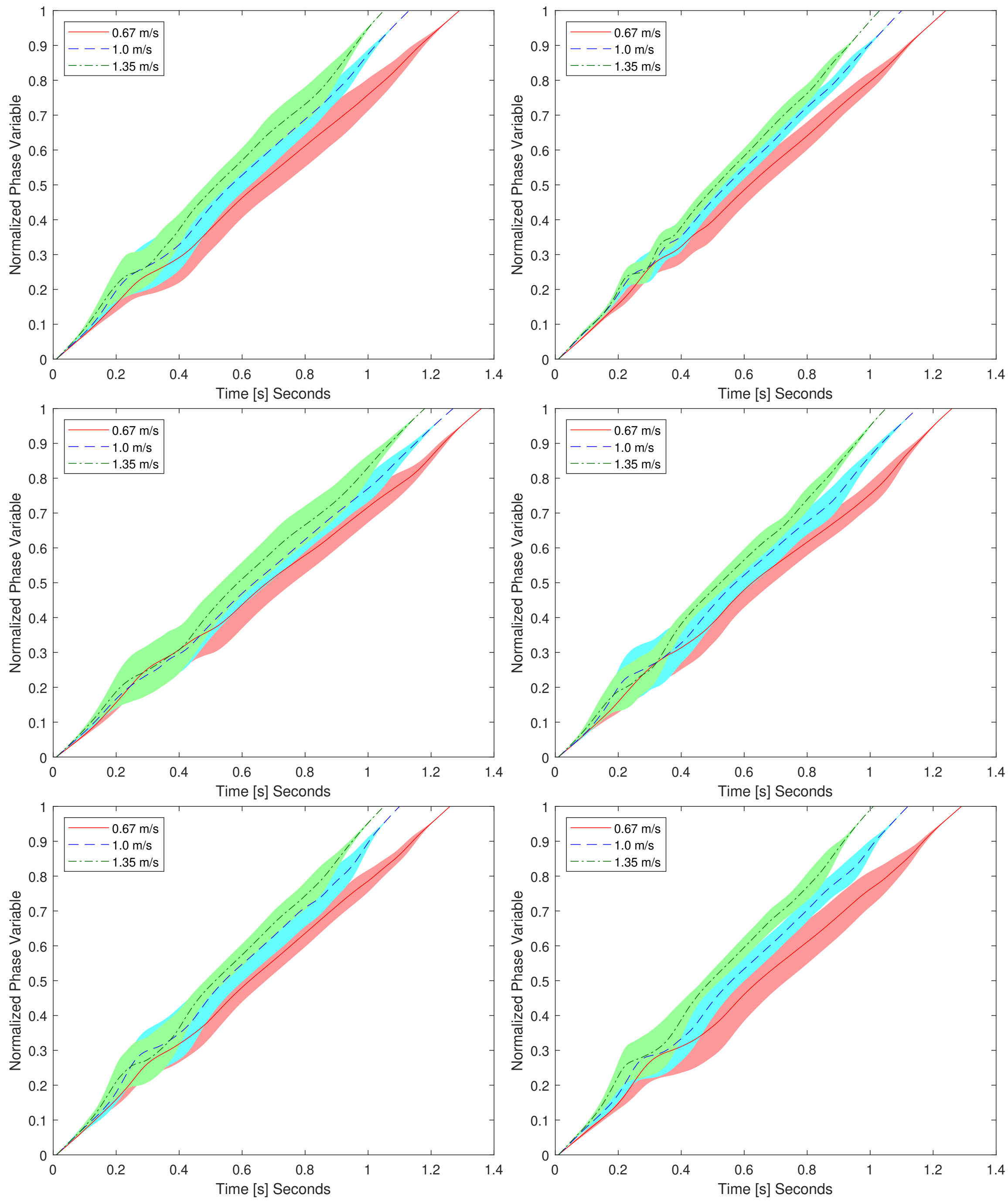

Figure 5.3: Reading from top to bottom, left to right normalized phase results for test subjects 1-6 walking at a 10 degree decline at the three different trial speeds. The lines provide the average normalized phase variable throughout the gait cycle, and the shaded region is the standard deviation over the 30-second trial period.

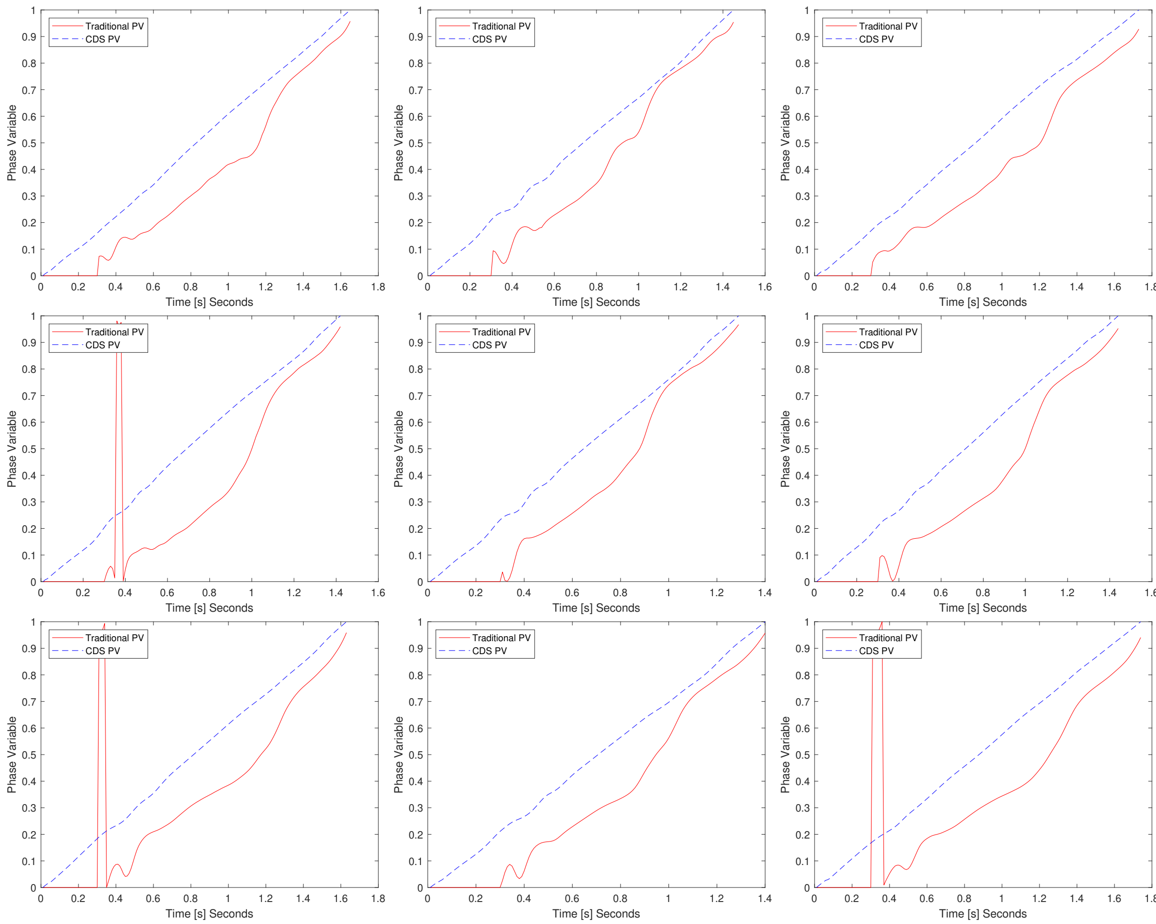

Figure 5.4: Reading from top to bottom, normalized phase results for test subjects 1-3 walking on level ground broken into three segments from left to right. The trial period represented by each row demonstrates a series of two transitions. Reading from left to right, the subject walks at 0.67 m/s in the left graph, then transitions to 1.35 m/s and back to 0.67 m/s in the right graph. Using two different calculations, each graph displays the average phase variable over 20 seconds of walking.

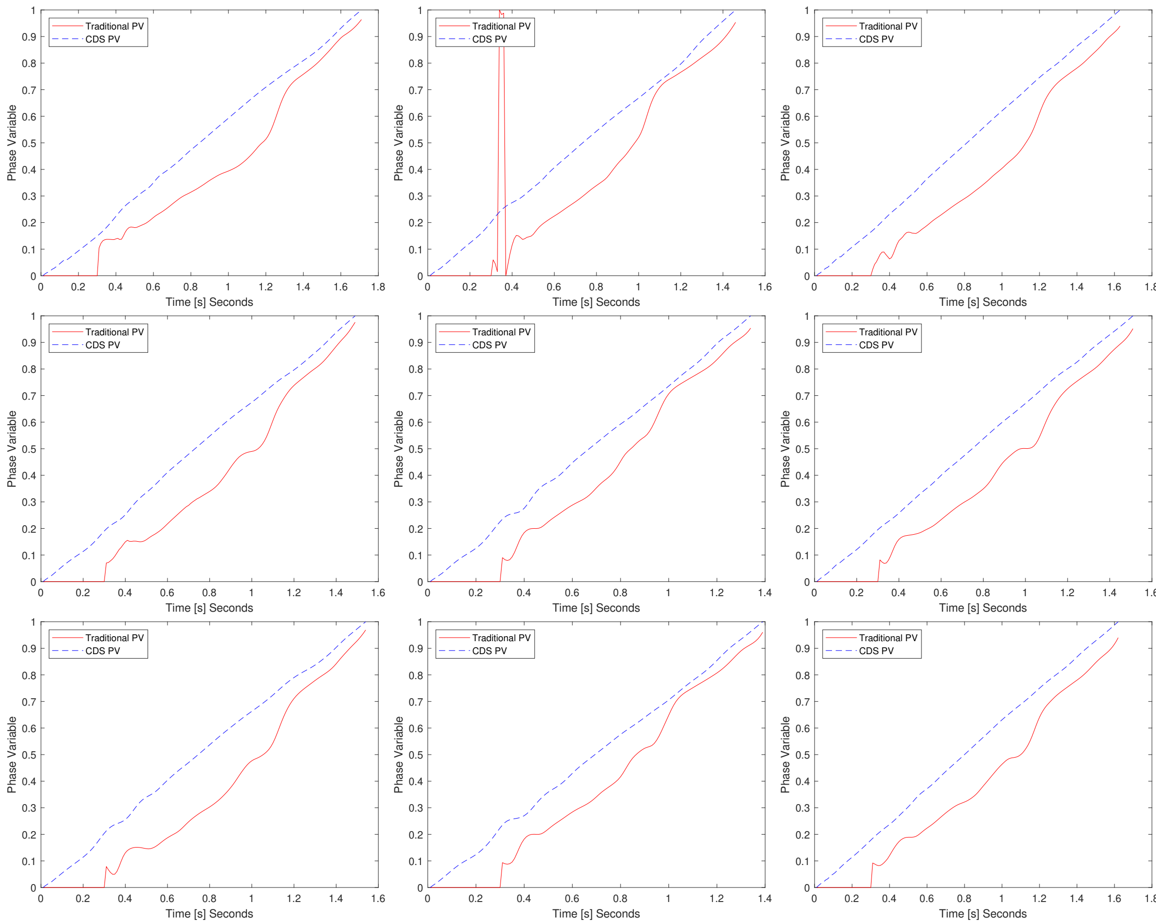

Figure 5.5: Reading from top to bottom, normalized phase results for test subjects 4-6 walking on level ground broken into three segments from left to right. The trial period represented by each row demonstrates a series of two transitions. Reading from left to right, the subject walks at 0.67 m/s in the left graph, then transitions to 1.35 m/s and back to 0.67 m/s in the right graph. Using two different calculations, each graph displays the average phase variable over 20 seconds of walking.

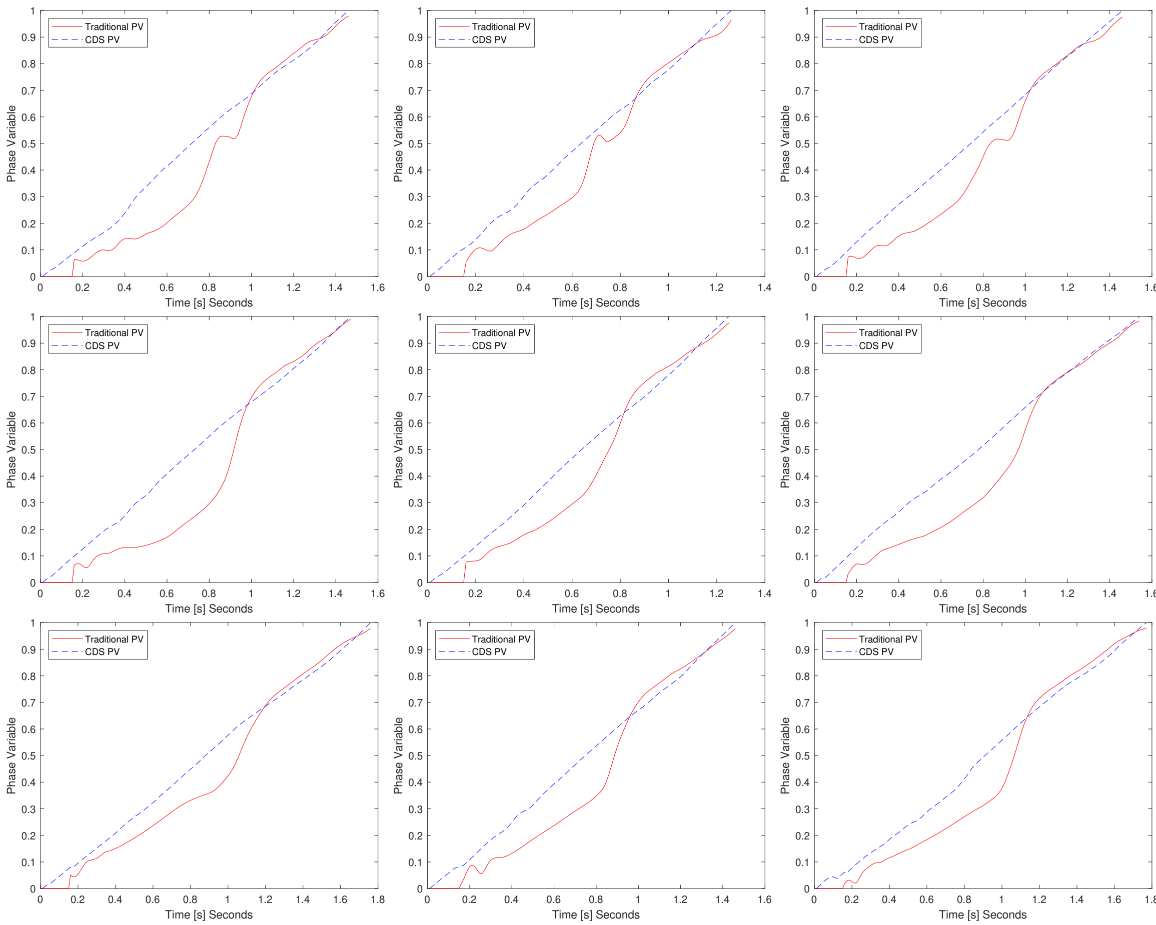

Figure 5.6: Reading from top to bottom, normalized phase results for test subjects 1-3 at walking on a 10-degree incline broken into three segments from left to right. The trial period represented by each row demonstrates a series of two transitions. Reading from left to right, the subject walks at 0.67 m/s in the left graph, then transitions to 1.35 m/s and back to 0.67 m/s in the right graph. Using two different calculations, each graph displays the average phase variable over 20 seconds of walking.

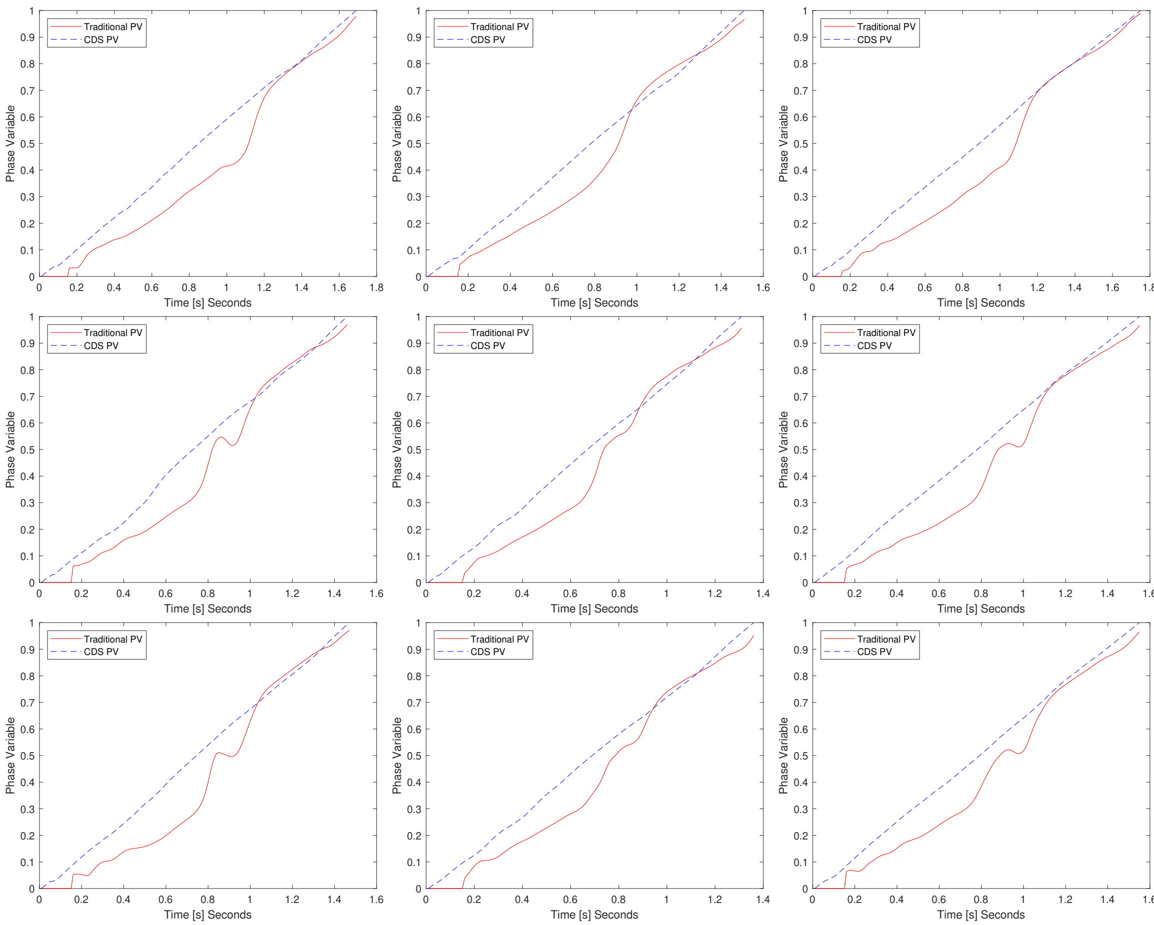

Figure 5.7: Reading from top to bottom, normalized phase results for test subjects 4-6 at walking on a 10-degree incline broken into three segments from left to right. The trial period represented by each row demonstrates a series of two transitions. Reading from left to right, the subject walks at 0.67 m/s in the left graph, then transitions to 1.35 m/s and back to 0.67 m/s in the right graph. Using two different calculations, each graph displays the average phase variable over 20 seconds of walking.

Chapter 6

Conclusions and Future Work

This thesis proposed a new method for calculating a human inspired phase variable for gait cycle parametrization. The discussion and results show an improvement to the original phase portrait method. The proposed method handles noisy input signals and unknown transitions during gait more effectively. The dynamic nature of the process also shows promise for addressing some of the more dynamic walking tasks, such as climbing or descending stairs.

A canonical dynamical system was leveraged as the backbone of the algorithm. The CDS combined a dynamic Fourier series to model the current state and an adaptive oscillator to extract the frequency and phase information. The CDS was combined with a dynamic time shift, allowing for a more robust and accurate input signal from the gyroscope. Although the thigh angular velocity was the input signal, the time shifting allowed the calculated phase variable to correspond to the thigh angle throughout the gait cycle. The phase variable could be converted to a real-time percentage to display the gait cycle percentage accurately.

Additionally, the improvements in the robustness of the phase variable calculations allowed for a more straightforward approach when designing an interface for human sensing. Small movements in the IMU caused by the subject completing walking tasks had little to no effect on the phase variable output. This reduced the complexity of the mounting mechanism to a simple case and Velcro strap. The design allowed for a versatile mount that could be used for a variety of subjects and a variety of different tests/conditions.

Ultimately, the work completed in this thesis provides a new solution to problems presented in section 1.2. The inspiration for this project was to improve the real-time control of wearable robotics such as a lower limb exoskeleton and full leg prosthesis. Both wearable devices needed continuous feedback from a simple sensing scheme to be aware of throughout the gait cycle. It was also crucial that the approach was time-invariant and assumptions about the gait were not made. Specifically, the CDS phase variable would provide a significant improvement when looking at the current control approach for the prosthesis. Increased awareness would allow the leg to adjust and dynamically match the user's gait more accurately. Further improvements to the work presented in this thesis will need to be made to finalize the design, but a functional prototype demonstrated the algorithm's effectiveness.

6.1 Future Work

Since this work focused on improving and developing a new phase variable calculation approach, there remains a significant improvement in the hardware implementation. Additionally, future work will include algorithm parameter tuning and testing other locomotion-based tasks. A breakdown of the specific improvements will be outlined in the following paragraphs.

Starting with the hardware improvements, the most apparent update would be transitioning from a general-purpose processor to something application specific. The Raspberry Pi is an excellent development tool but is not ideal for creating a more finalized product. The Raspberry Pi provides an excess of peripherals that are not being used and could be eliminated to reduce the size and power consumption of the microprocessor. Potential options for purchase would be the beagleboard PocketBeagle, Raspberry Pi Pico, or Arduino Pro Portenta. These processors will provide similar computing performance in Linux-based environments with a much smaller package and only the necessary communication peripherals. With this transition, there would also be a shift from using the MTi development board to simply interfacing the IMU directly with the processor. Again, This would reduce the system size and allow the processor and IMU to be mounted on a single board. The updated package size would also enable the subjects to wear the entire system on their thigh.

The following hardware improvement would be the use of an upgraded communication protocol. Currently, serial communication is used. The protocol was selected because the IMU could be easily interfaced with the Raspberry Pi using USB. A transition to serial peripheral interface (SPI) communication protocol would occur in future hardware implementation versions. SPI would increase communication speed and eliminate timing errors since a shared clock line exists. Adjustments in hardware and software would need to be made to use SPI communication protocol.

The last hardware update to be included in future work would be a portable power supply. In the current configuration, the IMU is tethered to the Raspberry Pi by a Micro-USB cable, and the Raspberry Pi is tethered to a confined space because of the need for an external power supply. The Raspberry Pi requires a 5.0V 3.0A (15 Watt) USB-C power supply. This power demand makes it difficult to use a portable battery as a power supply. Processors such as the PocketBeagle only require 5V 0.5A (2.5 Watts) of power. This power requirement will allow a smaller battery to be effectively used and integrated into the wearable sensing package. A smaller processor, no breakout board, and battery will transform the current version into a much smaller, wearable, and portable package.

The current algorithm has significantly improved the traditional approach, but there are still several steps for future improvement. The first algorithm-based improvement would be implementing a filter on the gyroscope input signal. Although the algorithm showed it could improve phase variable linearity with a noisy signal adding a simple filter to the input would provide marginal but additional improvement. A simple mean or moving average filter would further smooth the input signal and help remove any short-term overshoots or fluctuations. Additionally, with the aid of the 120 walking data sets, the algorithm could be rerun, and the initial parameters could be tuned to promote quicker frequency and phase convergence. Specifically, the number of Fourier Series coefficients, the learning coefficient, and the coupling constant could be further tuned.

Lastly, one of the most significant continuations for this project will be further testing on human subjects. Additional testing will help determine where adjustments in the algorithm need to occur. A focus will be made on testing a variety of different locomotion-based activities. Future tests could include but are not limited to ascending and descending stairs, starting and stopping motion throughout gait, dynamically changing inclines, and running. Increasing the number of tested tasks will allow for more educated improvements and confidence in the design for gait parameterization in an everyday environment.

Upon gaining confidence in the algorithm across various locomotion tasks, the system could be integrated with different wearable robots such as the lower limb exoskeleton and full leg prosthesis. Each project could request a desired phase variable input form to incorporate into the current control algorithms. The only additional requirement would be communication to transmit the calculated phase variable to the host in real time.

Appendices

Appendix A Additional Results

This appendix section presents additional results recorded during subject trials but not in the paper's main body. The additional results show phase variable calculations from walking trials at a 5-degree incline and decline. The same conclusions from the main body can be drawn when viewing these results.

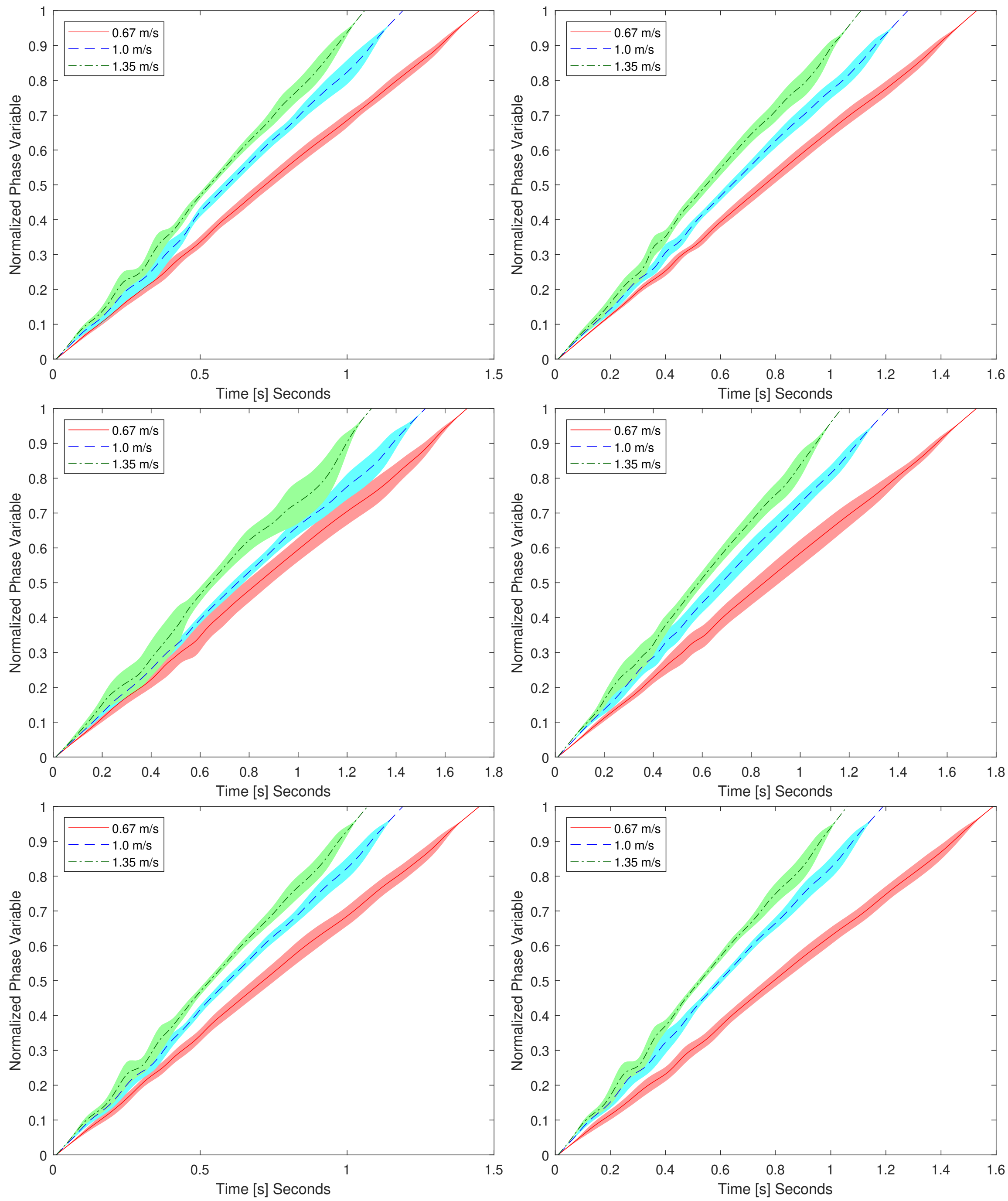

Figure 1: Reading from top to bottom, left to right normalized phase results for test subjects 1-6 walking at a 5 degree incline at the three different trial speeds. The lines provide the average normalized phase variable throughout the gait cycle, and the shaded region is the standard deviation over the 30-second trial period.

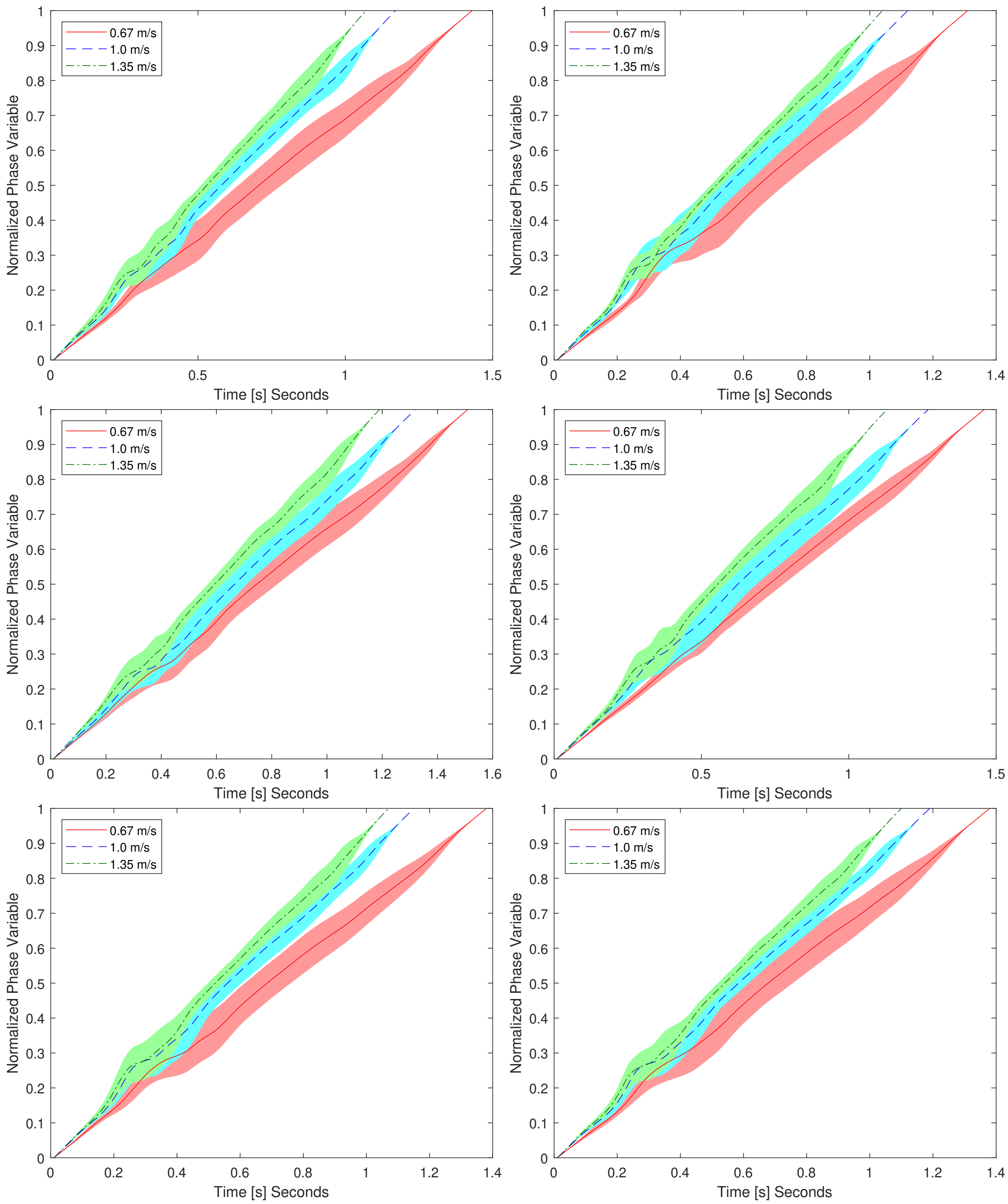

Figure 2: Reading from top to bottom, left to right normalized phase results for test subjects 1-6 walking at a 5 degree decline at the three different trial speeds. The lines provide the average normalized phase variable throughout the gait cycle, and the shaded region is the standard deviation over the 30-second trial period.

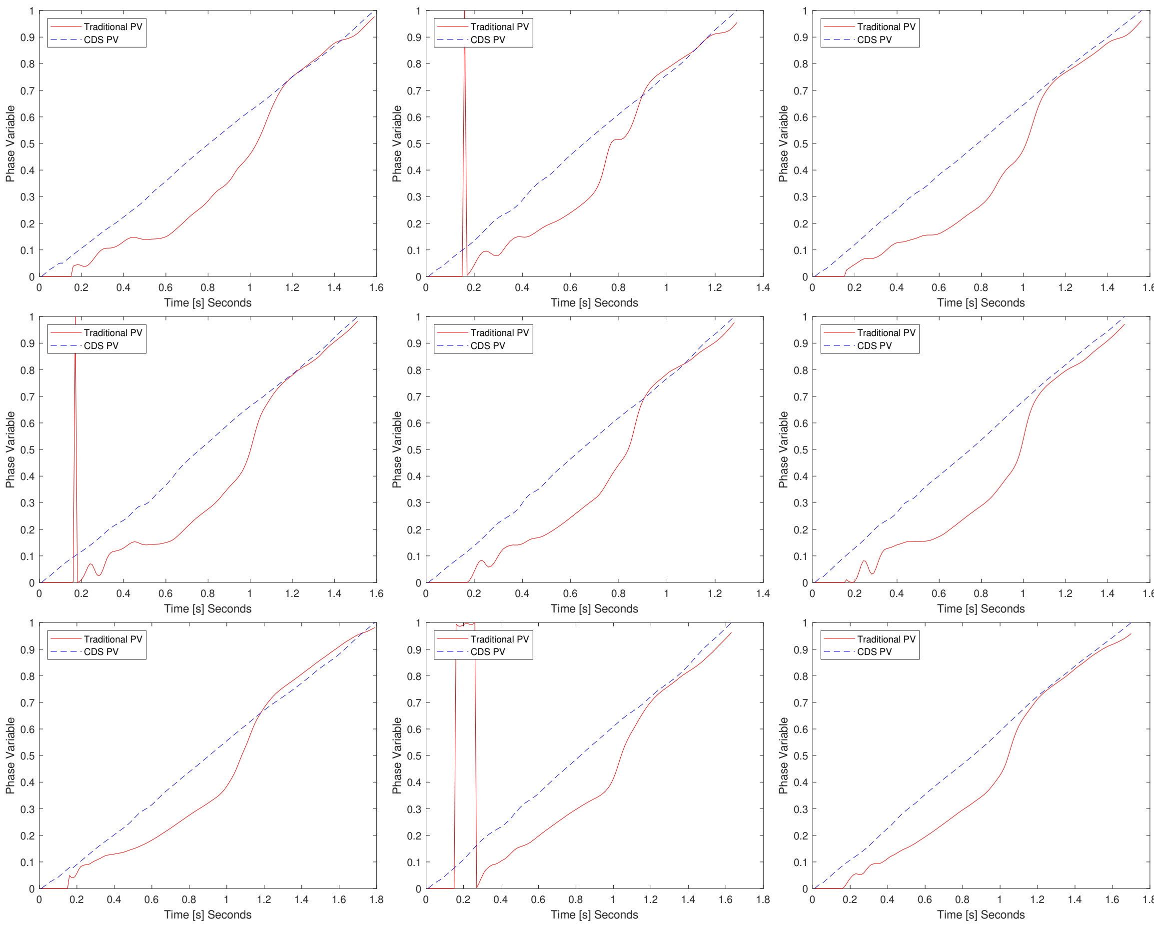

Figure 3: Reading from top to bottom, normalized phase results for test subjects 1-3 at walking on a 5-degree incline broken into three segments from left to right. The trial period represented by each row demonstrates a series of two transitions. Reading from left to right, the subject walks at 0.67 m/s in the left graph, then transitions to 1.35 m/s and back to 0.67 m/s in the right graph. Using two different calculations, each graph displays the average phase variable over 20 seconds of walking.

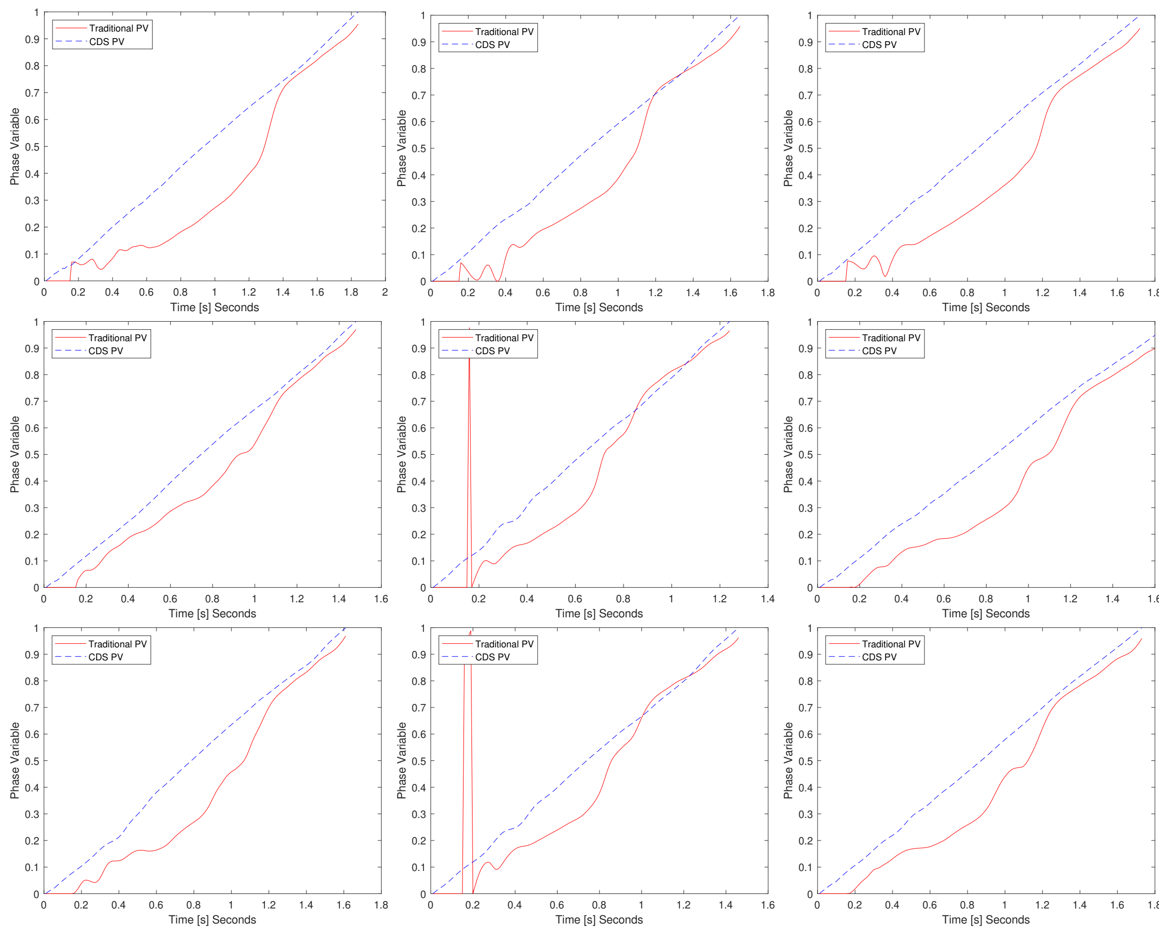

Figure 4: Reading from top to bottom, normalized phase results for test subjects 4-6 at walking on a 5-degree incline broken into three segments from left to right. The trial period represented by each row demonstrates a series of two transitions. Reading from left to right, the subject walks at 0.67 m/s in the left graph, then transitions to 1.35 m/s and back to 0.67 m/s in the right graph. Using two different calculations, each graph displays the average phase variable over 20 seconds of walking.

Appendix B Software Implementation

This appendix section provides source code for the software implementation of the proposed phase variable calculation algorithm.

```
def CDS_Setup(self):

    #Define the state variables and covariance
    self.T = 1/100 #Sampling frequency
    self.M = 7 #Number of Fourier series components
    self.eta = 1 #Learning Coefficient
    self.mu = 0.1 #Coupling Constant

    #Define initial frequency and phase variable
    self.w = [2*pi*2/5]
    self.phi = [0]

    self.ac = np.zeros(self.M)
    self.bc = np.zeros(self.M)
```

```
def CDS_Run(self, InputVal):

    y = InputVal
    self.estimate = 0

    for c in range(self.M):
        self.estimate = self.estimate + self.ac[c] * cos(c*self.phi[-1]) + self.
                                                   bc[c] * sin(c*self.phi[-1])

    self.error = y - self.estimate

    w_curr = self.w[-1]
    self.w.append(abs(w_curr - self.T*self.mu*self.error*sin(self.phi[-1])))

    for c in range(self.M):
        self.ac[c] = self.ac[c] + self.eta * self.T * cos(c*self.phi[-1])*self.
                                                   error
        self.bc[c] = self.bc[c] + self.eta * self.T * sin(c*self.phi[-1])*self.
                                                   error
```

```
phi_curr = self.phi[-1]
phi_next = (phi_curr + self.T*(w_curr - self.mu*self.error*sin(phi_curr))) %
                                                    (2*pi)

if(((phi_next - phi_curr) % (2*pi)) > (0.5*pi)):
    self.phi.append(phi_curr)
else:
    self.phi.append(phi_next)
```

Bibliography

[1] T. E. Parr, A. R. Hippensteal, and J. D. DesJardins, "Development of a length-actuated lower limb prosthesis: Functional prototype and pilot study," *JPO: Journal of Prosthetics and Orthotics*, 2022.

[2] A. Saboor, T. Kask, A. Kuusik, M. M. Alam, Y. Le Moullec, I. K. Niazi, A. Zoha, and R. Ahmad, "Latest research trends in gait analysis using wearable sensors and machine learning: A systematic review," *Ieee Access*, vol. 8, pp. 167 830–167 864, 2020.

[3] M. F. Shaikh, Z. Salcic, and K. Wang, "Analysis and selection of the force sensitive resistors for gait characterisation," in *2015 6th International Conference on Automation, Robotics and Applications (ICARA)*. IEEE, 2015, pp. 370–375.

[4] "Xsens MTi-7 GNSS/INS — Movella.com — movella.com," https://www.movella.com/products/sensor-modules/xsens-mti-7-gnss-ins, [Accessed 12-Jun-2023].

[5] "CanaKit Raspberry Pi 4 Case - Premium Black (High-Gloss) — canakit.com," https://www.canakit.com/raspberry-pi-4-case.html, [Accessed 13-Jun-2023].

[6] W. E. Harcourt-Smith, "The origins of bipedal locomotion," *Handbook of paleoanthropology*, vol. 3, pp. 1483–1518, 2007.

[7] D. Quintero, D. J. Lambert, D. J. Villarreal, and R. D. Gregg, "Real-time continuous gait phase and speed estimation from a single sensor," in *2017 IEEE Conference on Control Technology and Applications (CCTA)*. IEEE, 2017, pp. 847–852.

[8] S. Šlajpah, R. Kamnik, and M. Munih, "Kinematics based sensory fusion for wearable motion assessment in human walking," *Computer methods and programs in biomedicine*, vol. 116, no. 2, pp. 131–144, 2014.

[9] B. Toro, C. Nester, and P. Farren, "A review of observational gait assessment in clinical practice," *Physiotherapy theory and practice*, vol. 19, no. 3, pp. 137–149, 2003.

[10] J. Perry and J. M. Burnfield, "Gait analysis: Normal and pathological function."

[11] T. Petrič, A. Gams, A. J. Ijspeert, and L. Žlajpah, "On-line frequency adaptation and movement imitation for rhythmic robotic tasks," *The International Journal of Robotics Research*, vol. 30, no. 14, pp. 1775–1788, 2011.

[12] B. K. Higginson, "Methods of running gait analysis," *Current sports medicine reports*, vol. 8, no. 3, pp. 136–141, 2009.

[13] A. Pfister, A. M. West, S. Bronner, and J. A. Noah, "Comparative abilities of microsoft kinect and vicon 3d motion capture for gait analysis," *Journal of medical engineering & technology*, vol. 38, no. 5, pp. 274–280, 2014.

[14] T. Cloete and C. Scheffer, "Benchmarking of a full-body inertial motion capture system for clinical gait analysis," in *2008 30th Annual International Conference of the IEEE Engineering in Medicine and Biology Society*. IEEE, 2008, pp. 4579–4582.

[15] V. Cimolin and M. Galli, "Summary measures for clinical gait analysis: A literature review," *Gait & posture*, vol. 39, no. 4, pp. 1005–1010, 2014.

[16] W. Tao, T. Liu, R. Zheng, and H. Feng, "Gait analysis using wearable sensors," *Sensors*, vol. 12, no. 2, pp. 2255–2283, 2012.

[17] R. Takeda, S. Tadano, M. Todoh, M. Morikawa, M. Nakayasu, and S. Yoshinari, "Gait analysis using gravitational acceleration measured by wearable sensors," *Journal of biomechanics*, vol. 42, no. 3, pp. 223–233, 2009.

[18] Y. Hutabarat, D. Owaki, and M. Hayashibe, "Recent advances in quantitative gait analysis using wearable sensors: a review," *IEEE Sensors Journal*, vol. 21, no. 23, pp. 26 470–26 487, 2021.

[19] B. Zhang, S. Jiang, D. Wei, M. Marschollek, and W. Zhang, "State of the art in gait analysis using wearable sensors for healthcare applications," in *2012 IEEE/ACIS 11th International Conference on Computer and Information Science*. IEEE, 2012, pp. 213–218.

[20] T. L. Wu, A. Murphy, C. Chen, and D. Kulić, "Human-in-the-loop auditory cueing strategy for gait modification," *IEEE Robotics and Automation Letters*, vol. 6, no. 2, pp. 3521–3528, 2021.

[21] M. Kadaba, H. Ramakrishnan, M. Wootten, J. Gainey, G. Gorton, and G. Cochran, "Repeatability of kinematic, kinetic, and electromyographic data in normal adult gait," *Journal of orthopaedic research*, vol. 7, no. 6, pp. 849–860, 1989.

[22] G. Steinwender, V. Saraph, S. Scheiber, E. B. Zwick, C. Uitz, and K. Hackl, "Intrasubject repeatability of gait analysis data in normal and spastic children," *Clinical biomechanics*, vol. 15, no. 2, pp. 134–139, 2000.

[23] I. P. Pappas, T. Keller, S. Mangold, M. R. Popovic, V. Dietz, and M. Morari, "A reliable gyroscope-based gait-phase detection sensor embedded in a shoe insole," *IEEE sensors journal*, vol. 4, no. 2, pp. 268–274, 2004.

[24] A. Behboodi, H. Wright, N. Zahradka, and S. C. Lee, "Seven phases of gait detected in real-time using shank attached gyroscopes," in *2015 37th Annual International Conference of the IEEE Engineering in Medicine and Biology Society (EMBC)*. IEEE, 2015, pp. 5529–5532.

[25] A. U. Alahakone, S. A. Senanayake, and C. M. Senanayake, "Smart wearable device for real time gait event detection during running," in *2010 IEEE Asia Pacific conference on circuits and systems*. IEEE, 2010, pp. 612–615.

[26] R. T. Lauer, B. T. Smith, and R. R. Betz, "Application of a neuro-fuzzy network for gait event detection using electromyography in the child with cerebral palsy," *IEEE Transactions on Biomedical Engineering*, vol. 52, no. 9, pp. 1532–1540, 2005.

[27] D. J. Villarreal, H. A. Poonawala, and R. D. Gregg, "A robust parameterization of human gait patterns across phase-shifting perturbations," *IEEE Transactions on Neural Systems and Rehabilitation Engineering*, vol. 25, no. 3, pp. 265–278, 2016.

[28] T. Lenzi, M. C. Carrozza, and S. K. Agrawal, "Powered hip exoskeletons can reduce the user's hip and ankle muscle activations during walking," *IEEE Transactions on Neural Systems and Rehabilitation Engineering*, vol. 21, no. 6, pp. 938–948, 2013.

[29] S. Rossignol, R. Dubuc, and J.-P. Gossard, "Dynamic sensorimotor interactions in locomotion," *Physiological reviews*, vol. 86, no. 1, pp. 89–154, 2006.

[30] T. K. Best, C. G. Welker, E. J. Rouse, and R. D. Gregg, "Data-driven variable impedance control of a powered knee–ankle prosthesis for adaptive speed and incline walking," *IEEE Transactions on Robotics*, 2023.

[31] R. Heliot, R. Pissard-Gibollet, B. Espiau, and F. Favre-Reguillon, "Continuous identification of gait phase for robotics and rehabilitation using microsensors," in *ICAR'05. Proceedings., 12th International Conference on Advanced Robotics, 2005.* IEEE, 2005, pp. 686–691.

[32] R. P. . N. Group, "Python standalone library for use with the xsens imu," https://github.com/rpng/xsens_standalone, 2016, [Accessed 20-Jun-2023].